# Introduction

## Aims

This thesis is a structural and metamorphic study of multiply deformed and metamorphosed early-Proterozoic rocks comprising the Strangways Metamorphic Complex and Harts Range Group in the central Arunta Block, central Australia. The Arunta Block is an extensive (200 000 $km^2$), generally southeast-trending inlier of high-grade early- to mid-Proterozoic rocks that are unconformably overlain by mildly deformed late-Proterozoic to Phanerozoic sediments. The Strangways Metamorphic Complex and Harts Range group consist of folded granulite facies gneisses, granofelses and metasediments cut by north-dipping mylonite and schist zones. Alignments of minerals in kinematic fabrics from metamorphic tectonites record portions of their tectonometamorphic history. The morphology, composition and evolution of the mineral fabrics in the Strangways Metamorphic Complex and Harts Range Group are described, with the aims of: (1) determining the relative timing of deformation and metamorphic events; (2) deriving a pressure-temperature-time-deformation evolutionary path for the terrain; and (3) constructing models for the tectonic evolution of the central Arunta Block. The metamorphic and structural history of the Strangways Metamorphic Complex, the Harts Range Group and the shear zones, place constraints on the interpretation of the tectonometamorphic evolution of the central Arunta Block.

The geochemistry of rocks from the Strangways Metamorphic Complex is examined and used to interpret the early-Proterozoic tectonic setting in which precursors were formed. Whole-rock geochemistry can also indicate the possible effects of alteration consequent on fluid movement during diagenesis and metamorphism/deformation.

The geochemistry and tectonometamorphic evolution of a regional high-grade belt, such as the central Arunta Block, provides an insight into processes of crustal formation, deformation and exhumation. However, the thermobarometric history and geochemistry of Proterozoic granulite terrains is generally not easy to reconcile with tectonic processes in Phanerozoic rocks and plate tectonic models. Many Proterozoic granulite terrains preserve evidence for very high heat fluxes during peak metamorphism, synchronous with compressional deformation. Models for Proterozoic orogenesis must accommodate a high heat flux, most probably as a result of lithospheric thinning, with synchronous crustal shortening (Loosveld and Etheridge, 1990), even though there appear to be no modern analogues. This thesis presents field, mineralogical and geochemical data, which provide constraints on the structural and metamorphic evolution of the central Arunta block and provide a basis for deducing the crustal and lithospheric processes that were responsible for deformation and metamorphism in the early- to mid-Proterozoic.

Deformation and metamorphic processes in the crust and mantle lithosphere may have a profound influence on the topography, erosion rate and deposition at the surface of the earth. The depositional history of mid-Proterozoic quartzose rocks comprising the Reynolds Range Group, in the northern Arunta Block, is interpreted to help determine the geometry of the mid-Proterozoic shelf and coastline that may have been influenced by the tectonic evolution of the central Arunta Block.

## Thesis Outline

Field mapping of the Strangways Metamorphic Complex and the Harts Range was undertaken using 1:25,000 colour aerial photos and compiled onto regional geological maps. Relevant field maps are presented in the text, where appropriate. All structural data are related to true north. The results of research work for this thesis have been presented as a series of papers to international journals. The relevant references are given at the end of the thesis, and individual Chapters largely follow the outline of the submitted papers.

The geochemistry of some unusual K-poor felsic granofels and gneisses in the Strangways Metamorphic Complex is described in Chapter 1. The anomalous whole-rock geochemistry of these samples may reflect heterogeneous alteration during diagenesis. The composition of retrograde minerals and depletion of yttrium are probably due to fluid movement after peak metamorphism. The whole-rock geochemistry of other gneisses in the Strangways Metamorphic Complex and an interpreted tectonic setting for development of the Strangways Metamorphic Complex protoliths are also briefly described in Chapter 1. A paper based on Chapter 1 has been accepted for publication in *Journal of Metamorphic Geology* (Norman and Flood, 1991).

The structural evolution of the Strangways Metamorphic Complex is described in Chapter 2. Five major deformations are recorded by rocks in the Strangways Metamorphic Complex. The Complex is interpreted as having undergone a major progressive non-coaxial reworking at granulite facies conditions after the metamorphic peak.

A general introduction to the metamorphic evolution of the Strangways Metamorphic Complex is presented in Chapter 3. This chapter presents evidence that two distinct metamorphic events ($M_1$ and $M_2$), distinct and different P-T conditions, affected the Strangways Metamorphic Complex. Pressure-temperature (P-T) estimates of the metamorphic conditions are given and the two events are related temporally to the structural evolution presented in Chapter 2. This Chapter is part of a published paper in *Journal of Structural Geology*, **12**, 667-684 (Norman and Clarke, 1990) and a conference abstract (Norman et al., 1989).

In Chapter 4, evidence for the metamorphic evolution of the Strangways Metamorphic Complex is more precisely defined. Pressure-temperature-time (P-T-t) paths for the Strangways Metamorphic Complex and Harts Range Group are derived using equilibrium mineral assemblages and mineral zoning in rocks from the two terrains. The derived P-T-t paths have important implications for constructing a tectonic

model. A paper based on this Chapter has been submitted for publication to *Precambrian Research* (Norman and Vernon, 1991).

The geometry and mineral compositions of ultramylonite zones dissecting the Strangways Metamorphic Complex and postdating $M_2$ are described in Chapter 5. Estimates of P-T conditions during ultramylonitization are similar to those obtained for $M_2$. The ultramylonite zones preserve a normal sense of shear and may represent post-compressional extension. A paper based on this Chapter has been submitted for publication to *Tectonophysics* (Norman and Vernon, 1991). This chapter also forms part of a conference abstract (Norman, 1989).

A paper on the depositional history of the Reynolds Range Group and the geometry of the mid-Proterozoic shelf has been submitted to *Precambrian Research* (Dirks and Norman, 1991). This paper is presented in the Appendix at the end of the thesis. The Reynolds Range Group crops out 250 km west of the Harts Range Group and unconformably overlies similar rocks to those of the Strangways Metamorphic Complex. Deposition of the Reynolds Range Group occurred at about the same time or slightly after peak metamorphism in the Strangways Metamorphic Complex (~1800 Ma ago) and reflects geometry of major structures and in the underlying rocks. The structural and metamorphic history of the Strangways Metamorphic Complex and Harts Range Group together with the depositional history of the Reynolds Range Group, provide the basis for interpreting the tectonic history of the central Arunta Block.

A synthesis of events affecting the Strangways Metamorphic Complex and Harts Range Group is used in Chapter 6 to interpret the structural and metamorphic evolution of the central Arunta Block. Structural and metamorphic data from rocks adjacent to the Amadeus Basin and shear zones separating the Strangways Metamorphic Complex and Harts Range Group are incorporated in this synthesis.

## Regional Geology

The Arunta Block (Noakes, 1953) is a 200 000 $km^2$ inlier of multiply deformed and metamorphosed early- to mid-Proterozoic rocks that is unconformably overlain by mildly deformed late-Proterozoic to Phanerozoic intracratonic basin sediments (Fig. 1.0). The Arunta Block has been subdivided into three tectonic provinces and three tectonostratigraphic divisions (Shaw et al., 1984a; Stewart et al., 1984) that display a broad upward increase in rock-type maturity. Interlayered felsic and mafic rocks mostly comprise the oldest rocks (Division 1), which are overlain by Division 2 metasediments. Quartzose platform sediments comprise the youngest rocks (Division 3) and unconformably overlie Division 2 metasediments. The Divisions have been interpreted as representing a three-stage evolution: bimodal volcanism in an ensialic rift setting, flysch-like sedimentation and quartzose platform sedimentation (Stewart et al., 1984, Shaw et al., 1984a). The Arunta Block was pervasively deformed and metamorphosed prior to being dissected by shear zones. Successive mineral assemblages have been interpreted as reflecting near-isobaric cooling at mid-crustal depths, until uplift and erosion some time before the deposition of the unconformably overlying late-Proterozoic basin sediments (Warren, 1983a; Warren and Stewart, 1988).

The intrusion of meridional-trending 1100-900 Ma mafic dykes throughout the Arunta Block (Black et al., 1980) and emplacement of the Mordor Igneous Complex (1180 Ma) south of the Strangways Metamorphic Complex (Nelson et al., 1989) may have coincided with extension and uplift that initiated formation of basins into which sediments of the Amadeus, Ngalia, Wiso and Georgina Basins were deposited. Significant displacement of the Arunta Block along ductile faults occurred during the mid-Carboniferous Alice Springs Orogeny (Stewart, 1971; Collins and Teyssier, 1989) that coincided with deposition of the Brewer Conglomerate in the the Amadeus Basin (Forman et al., 1967) and the development of south-verging nappes on the northern margin of the Amadeus Basin (Forman, 1971; Majoribanks, 1976).

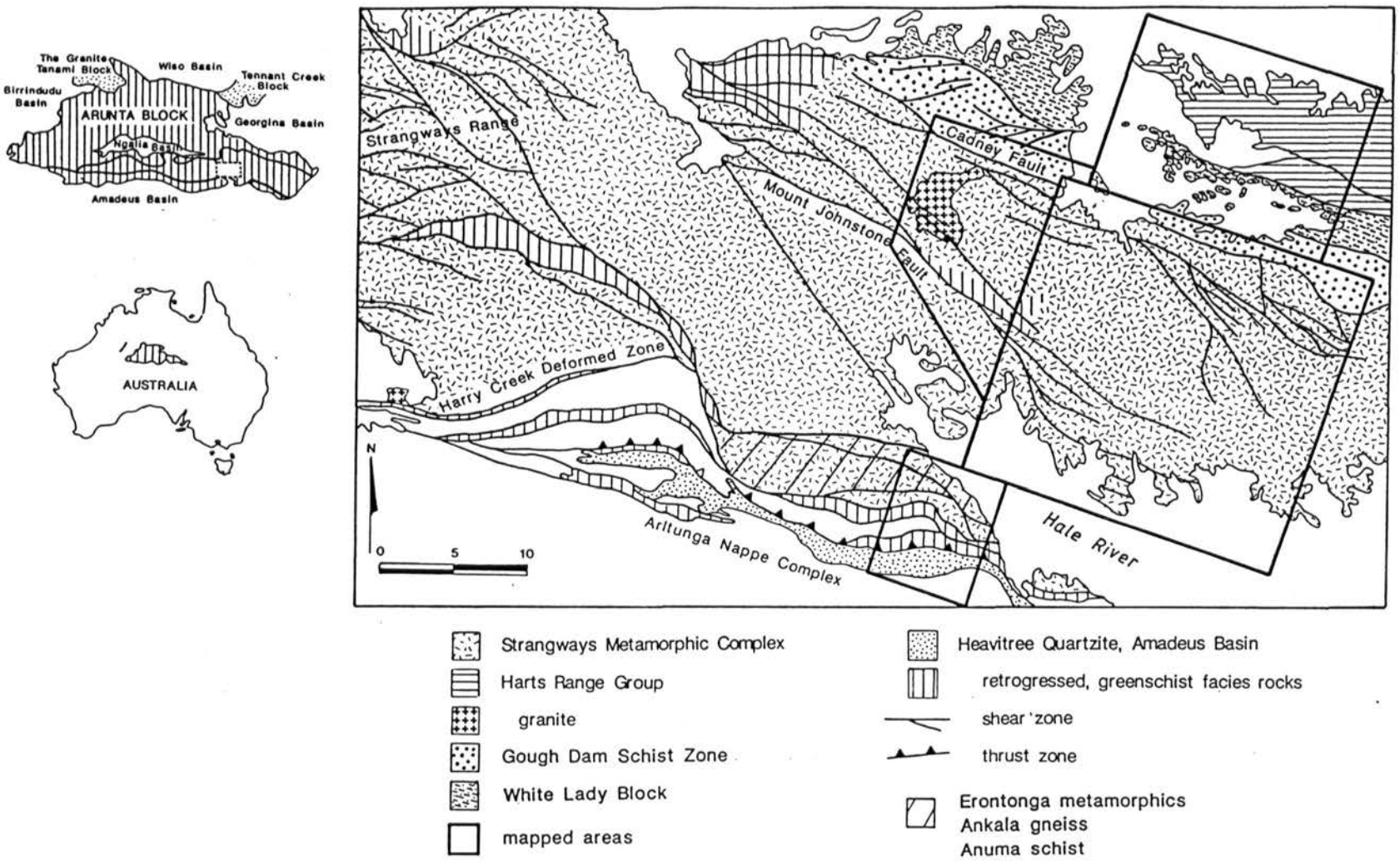


**Fig. 1-0** Regional geology of the central Arunta Block (after Shaw et al., 1983) showing areas mapped in detail.

The main area under investigation in this thesis is situated about 100-150 km northeast of Alice Springs, in the central tectonic province of the Arunta Block (Fig. 1.0). The first regional mapping of the this area was by Joklik (1955), who used the term "Harts Range Group" for all the rocks north of the Hale River. However, following Shaw et al. (1984b), the study area is divided into two major groups separated by north-dipping mylonite zones: the *Strangways Metamorphic Complex* in the south and the *Harts Range Group* in the north (Fig. 1.0). The Strangways Metamorphic Complex and the Harts Range Group are broadly equivalent to the Strangways Orogenic Belt and Harts Range Cover, respectively, of Ding and James (1985) and James and Ding (1988) who worked to the east of the area. The Strangways Metamorphic Complex belongs to the lowermost Division 1 rocks of Stewart et al. (1984) and the Harts Range Group belongs to the stratigraphically higher Division 2 rocks. Division 1 and 2 rocks are unconformably overlain by Division 3 platform sediments east of Alice Springs (Mawer 1980, 1983; Teyssier et al., 1988) and in the northern Arunta Block (Stewart et al., 1980; Dirks, 1991). The *Reynolds Range Group* crops out 150 km north of Alice Springs (Fig. AA.1, Appendix) and forms part of the Division 3 rocks. The depositional history of the Reynolds Range Group sediments is included as part of this thesis because no Division 3 sediments crop out in the main study area.

## Strangways Metamorphic Complex

The Strangways Metamorphic Complex is thought to record the earliest recognized metamorphic event in the Arunta Block, namely 1790±35 Ma (Rb-Sr data, Black et al., 1983), which affected rocks with a crustal formation age of about 2000 Ma, based on a Nd-Sm model age (Windrim and McCulloch 1986). Evidence for an isotopic disturbance at about 1800 Ma has been found elsewhere in the Arunta Block (Iyer et al 1976, Black et al 1983, Allen and Stubbs, 1982) and has been interpreted as a widespread granulite facies episode called the Strangways Event (Black et al., 1983).

The Strangways Metamorphic Complex was multiply deformed and metamorphosed at granulite facies conditions before being extensively dissected by

mylonite and retrograde shear zones (Shaw et al., 1979; Shaw et al., 1984b; Shaw and Langworthy 1984). Warren (1982, 1983a) estimated that peak metamorphism in the Strangways Metamorphic Complex occurred at conditions of P~8 kbar and T~850°C and suggested an anticlockwise P-T-t path involving isobaric cooling until the rocks were uplifted during the late-Proterozoic and again during the mid-Carboniferous Alice Springs Orogeny. However, Norman and Clarke (1990; Chapter 3) estimated that peak metamorphism ($M_1$) occurred at low pressure conditions (5-6 kbar) and that a second distinct 'up-pressure' metamorphic event ($M_2$) occurred after peak metamorphism. They also suggested that the increase in pressure during the second metamorphic event may have been synchronous with a major folding event (Chapter 2), which produced the macroscopic fold pattern in the Strangways Metamorphic Complex. This major folding event is interpreted as a progressive non-coaxial deformation at granulite facies conditions and is probably equivalent to what has been interpreted as ductile Proterozoic reworking in rocks from the Strangways Range, 75 km northwest of this study, by Goscombe (1991). An episode of ultramylonitization formed discrete, discontinuous shear zones that cut the pervasive tectonic fabrics in the Strangways Metamorphic Complex (Chapter 5). Although these shear zones mostly post-date macroscopic folding, the ultramylonite deformation predates deformation in the Gough Dam Schist Zone, which bounds the Strangways Metamorphic Complex to the north (Fig. 1.0).

The shear zones subdivide the Strangways Metamorphic Complex into a number of spatially-independent, morphological units, some of which are described in this thesis. The *Ongeva granulites* (after Shaw et al., 1984b) crop out in the northeast of the mapped area (Fig. 1.0) and the *Anamarra granite domain* crops out in the northwest of the mapped area (Norman and Clarke, 1990). To the south, in the Hale River, a wide zone of epidote-muscovite-rich mylonites separate the Ongeva granulites from the *Erontonga metamorphics*, *Ankala gneiss* and *Anuma schist* (Shaw et al., 1984b), which crop out along the northern margin of the Amadeus Basin. The geology of each of these units is briefly described below.

*Ongeva granulites*

The Ongeva granulites consist predominantly of interlayered quartzofeldspathic gneisses and two-pyroxene mafic granofelses, with minor intercalated metapelitic gneisses, calc-silicate rocks and rare marble. A mesoscopic variation in bulk rock composition is defined by cm to m-scale layers, which may reflect a primary sedimentary layering, although they have been commonly boudinaged due to tectonic deformation. The geochemistry of the Ongeva granulites has been interpreted as reflecting a bimodal suite of volcanics and altered tephras and tuffs that were produced in a rifted continental margin or intra-cratonic rift environment (Shaw et al., 1979; Stewart et al., 1984; Norman and Flood, 1991; Chapter 1). The felsic gneisses have rhyolitic compositions and the mafic gneisses have tholeiitic compositions (Shaw et al., 1979; 1984b; Warren and Shaw, 1985; Chapter 1).

Felsic and mafic orthogneisses are interlayered with supracrustal rocks. All rocks contain a well-developed gneissosity, which is defined by coarse-grained, mm to cm-scale leucosome layers that are generally sub-parallel to compositional boundaries but may locally be oblique. This gneissic foliation is folded by northeast-plunging, open to isoclinal inclined folds that produce the macroscopic fold pattern (Fig. 2.4). A well developed mineral elongation and stretching lineation is commonly parallel to the fold axes. These folds are generally cut by east-trending ultramylonite zones, which have a consistent north-side down sense of shear and have mineral compositions indicative of granulite facies conditions (Norman and Vernon 1991; Chapter 5). The ultramylonite zones appear to extend into the Anamarra granite domain to the west.

*Anamarra granite domain*

The Anamarra granite domain is distinguished from the Ongeva granulites by the presence of deformed megacrystic granite and calc-alkaline metagabbro The largest intrusion in the Anamarra granite domain is the Anamarra Granite (Shaw and Langworthy, 1984). However, the outcrop pattern and mesoscopic layering in the

Anamarra granite domain are generally very irregular and disrupted by wide zones of phyllonite and biotite schist, which are commonly retrogressed to greenschist facies assemblages. Between the wide phyllonite zones the Anamarra granite domain contains blocks of folded and interlayered quartzofeldspathic gneisses, mafic granofelses and minor cordierite gneisses, which are similar to gneisses in the Ongeva granulites. The interlayered high-grade gneisses contain a tectonometamorphic gneissosity similar to that in the Ongeva granulites, which is defined by coarse-grained, mm to cm-scale leucosome layers and is generally sub-parallel to compositional boundaries. Mesoscopic north-east plunging folds similar to those in the Ongeva granulites have also been recognized. The Anamarra Granite contains a northeast-trending magmatic foliation defined by aligned megacrysts, which is cut by east-trending mylonite zones continuous with shear zones in the surrounding gneisses.

Two phyllonitic shear foliations enclose the meta-igneous rocks and high-grade gneissic blocks. One is a steep north-trending shear foliation and the other is an east-trending north-dipping shear foliation. The north-trending foliation is commonly crenulated and bends into the cross-cutting east-trending shear foliation. The east-trending shear foliation appears to be continuous with ultramylonite zones in the Ongeva granulites. In the northern part of the Anamarra granite domain, both the north- and east-trending phyllonitic foliations contain a quartz stretching lineation and the rocks show evidence of a north-side up sense of shear that was probably produced during movement in the Gough Dam Schist Zone, which bounds the Anamarra granite domain (Fig. 1.0). Coarse-grained pegmatites, veins of epidote and quartz, and meso-faults cut the phyllonitic foliations in the Anamarra granite domain and are probably related to late fluid movement and deformation.

The Anamarra granite domain probably represents an extension of the Ongeva granulites that was intruded by an igneous complex after peak metamorphism, but before the main macroscopic folding event or ultramylonitization. The boundary between the

Anamarra granite domain and the Ongeva granulites is not well defined because of subsequent deformation and retrogression along phyllonitic shear zones.

*Erontonga metamorphics and Ankala gneiss*

The Erontonga metamorphics and the Ankala gneiss crop out between the Hale River and the deformed northern margin of the Amadeus Basin (Fig. 1.0). They consist of quartzofeldspathic gneisses, mafic gneisses, metapelitic gneisses and calc-silicate rocks. A gneissic foliation in the Erontonga metamorphics and Ankala gneiss is cut by a well-developed, pervasive north-dipping biotite foliation that contains a steep northeast-plunging stretching lineation. Asymmetric and oblique mineral fabrics indicate that the biotite foliation was produced during south-directed shearing. Greenschist facies retrogression is common, particularly near the deformed sediments of the Amadeus Basin, and was probably related to deformation of the Amadeus Basin during the mid-Carboniferous Alice Springs Orogeny. The effects of the Alice Springs Orogeny are characterized by the development of a new mineral foliation and lineation in the Erontonga metamorphics and the Ankala gneiss, which is texturally distinct from the pervasive biotite foliation and lineation (Chapter 6).

*Anuma schist*

The Anuma schist is a coarse-grained biotite schist that contains sillimanite, kyanite, staurolite and fine-grained white mica. It crops out on the northern margin of the Erontonga metamorphics and contains a white-mica elongation lineation oblique to a steep high-grade mineral elongation lineation. The oblique lineation is subparallel to mineral elongation lineations in the Erontonga metamorphics and Ankala gneiss adjacent to the Amadeus Basin, which are characteristic of deformation in the Alice Springs Orogeny.

## Harts Range Group

The Harts Range Group consists of interlayered and folded, garnet-bearing mafic gneisses, metapelitic gneisses, calc-silicate rocks and quartz-rich gneisses, which are cut by north-dipping mylonite zones that preserve a south-directed sense of shear. The mylonite zones are commonly parallel to the lithological layering and may contain zones of extensive retrogression. Mylonitic deformation post-dated high-grade metamorphism and upright folding of the Harts Range Group (Chapter 6).

The Harts Range Group has been divided into the *Harts Range meta-igneous complex and the Irindina supracrustal assemblage*, which have been interpreted as suites of metamorphosed basic igneous rocks and volcano-sedimentary rocks that formed in a rifted continental margin or intra-cratonic rift environment (Sivell and Foden, 1985). The Harts Range Group has been interpreted as a supracrustal sequence produced during an episode of crustal extension that involved the 'basement' Strangways Metamorphic Complex (Ding and James, 1985; Sivell and Foden, 1985). On the basis of geochemical analyses of rocks from the Harts Range meta-igneous complex, Sivell (1988) inferred two separate phases of mafic magmatism. Early magmatism was characterized by rocks of continental tholeiitic compositions and later magmatism was characterized by normal tholeiitic compositions resembling rocks from convergent plate margin settings (Sivell, 1988). Sivell (1988) suggested that this change in rock composition was indicative of a change from extensional to compressional tectonics. However, andesites, which are distinctively associated with convergent plate boundaries (e.g. Gill, 1981), have not been found in the Harts Range meta-igneous complex.

Upright folding of the Harts Range Group produced east-west trending, tight to isoclinal, macroscopic folds with shallow plunges and an inferred northnortheast shortening axis. Mylonitization postdated folding and it has been suggested that reactivation of a major extensional detachment zone was responsible for southward

thrusting of the the Harts Range group onto the Strangways Metamorphic Complex (Ding and James, 1985; James and Ding, 1988).

In this thesis, it is proposed that the Harts Range group and the Strangways Metamorphic Complex formed part of the same protolith that was simultaneously deformed during a major Proterozoic tectonometamorphic event (Chapter 4, Chapter 6).

**Gough Dam Schist Zone and the White Lady Block**

The Gough Dam Schist Zone crops out on the northern margin of the Strangways Metamorphic Complex and consists of phyllonitic quartzofeldspathic gneisses, biotite schists and residual pods of the Strangways Metamorphic Complex. (Fig. 1.0). The Gough Dam Schist Zone contains a quartz rodding and a biotite±sillimanite elongation lineation that plunges to the northnortheast. Kyanite and gedrite-anthophyllite assemblages have been described from similar phyllonitic zones to the west by Warren (1983a).

The White Lady Block (Shaw et al., 1984b) crops out to the north of the Gough Dam Schist Zone (Fig. 1.0) and consists of anastomosing, north-dipping ultramylonite zones and pods of mafic gneisses, quartzofeldspathic gneisses, sillimanite gneisses and minor megacrystic gneisses, similar to gneisses in the Strangways Metamorphic Complex.

The Gough Dam Schist Zone and ultramylonite zones in the White Lady Block preserve evidence for south-directed shearing that may have been responsible for juxtaposing the Harts Range Group (Fig. 1.0) against the Strangways Metamorphic Complex (Ding and James 1985, James and Ding 1988). James and Ding (1988) have suggested that a major crustal detachment between the Harts Range Group and the Strangways Metamorphic Complex was active when the Bruna Gneiss was intruded at 1747 Ma (Mortimer et al., 1987). However, Collins and Teyssier (1989) have interpreted deformation in the Bruna Gneiss and other shear zones between the Harts Range and the Amadeus Basin, to the south, to be part of a crustal-scale Palaeozoic

deformation that produced the Arltunga Nappe Complex during the Alice Springs Orogeny in the mid-Carboniferous (Stewart, 1971). In this thesis, it is suggested that shearing in the Gough Dam Schist Zone and the White Lady Block represents a continuation of a major orogenic cycle in the Strangways Metamorphic Complex and the Harts Range Group, which probably occurred during the mid-Proterozoic (Chapter 6).

Areas of pervasive greenschist facies retrogression cut the Gough Dam Schist Zone and the White Lady Block. Chlorite and muscovite-epidote foliations cut the pervasive biotite foliation in the Gough Dam Schist Zone and commonly have a very oblique to subhorizontal mineral elongation. Microscopically, chlorite and muscovite appear to have replaced the original biotite. Greenschist facies retrogression was probably related to fluid movement and deformation during uplift of the central Arunta Block.

**Reynolds Range Group**

Within the Arunta Block at least two episodes of sedimentation alternated with widespread orogenic events (Stewart et al., 1984; Shaw et al., 1984a). The first depositional episode produced Division 1 and 2 rocks, such as the Strangways Metamorphic Complex and the Harts Range Group. The last depositional episode occurred between 1820 Ma and 1760 Ma (Dirks and Wilson, 1990; Collins et al., 1991) and resulted in the deposition of a conformable sequence of mature quartz-arenites, mudstones, carbonates and felsic volcanics comprising the Reynolds Range Group (Stewart et al., 1980; Dirks, 1991; Appendix).

The Reynolds Range Group crops out about 150 km north of Alice Springs in the northern tectonic province (Shaw et al., 1984a). It is highly deformed and metamorphosed from greenschist facies (500°C, 4-5 kbar; Dirks and Wilson, 1990) in the northwest to granulite facies (750°C, 4-5 kbar; Clarke and Powell, 1991) in the southeast. In the northwest, the Reynolds Range Group overlies Division 2 rocks of the the Lander Rock beds with an angular unconformably (Shaw et al., 1984a).

Sedimentary structures and bedforms are generally well preserved in the quartz-arenite and interbedded siltstone, mudstone and carbonate of the greenschist facies regions. However, in the granulite facies terrain, sedimentological detail has largely been obliterated by recrystallization.

The Reynolds Range Group has been deformed into a series of southeast-trending upright, tight to isoclinal folds and dissected by southeast-trending mylonite zones (Dirks and Wilson, 1990). U/Pb isotopic studies of zircon suggest that a granulite facies metamorphism, affecting the Reynolds Range Group, occurred at about 1730 Ma (Clarke et al., 1990; Collins et al., 1991). This metamorphism was probably synchronous with upright folding that produced the macroscopic fold pattern in the Reynolds Range (Dirks and Wilson, 1990). Mylonitic deformation and retrogression to greenschist facies assemblages in retrograde shear zones postdated folding.

Deformation in the Reynolds Range Group has a similar style to deformation in the Harts Range Group. In this thesis, a tectonic model is considered (Chapter 6), which involved a major widespread orogenic event that deformed and metamorphosed a large portion of the Arunta Block.

**Mineral abbreviations used in figures and tables** (after Kretz, 1983)

Ab- albite; Adr- andradite; An- anorthite; Alm- almandine; And- andalusite; Ann- annite; Ath- anthophyllite; Bt- biotite; Chl- chlorite; Cpx- clinopyroxene; Crd- cordierite; east- eastonite; en- enstatite; Ep- epidote; Fcrd- Fe cordierite; Fs- ferrosilite; Grt- garnet; Ged- gedrite; Grs- grossularite; Hc- hercynite; Hbl- Hornblende; Ilm- ilmenite; Kfs- K-feldspar; Kfs- K feldspar; Ky- kyanite; Mei- meionite; Mag- magnetite; Mgts- Mg-Tschermak; Ms- muscovite; Naph- Na phlogopite; Or- orthoclase; Opx- orthopyroxene; Phl- phlogopite; Pl- plagioclase; prp- pyrope; Qtz- quartz; Spr- Sapphirine; Scp- scapolite; Sil- sillimanite; Spl- spinel; St- staurolite; Wo- wollastonite; Zo- zoisite

# *CHAPTER 1*

# Geochemistry and structure of a K-poor felsic granofels in the Strangways Metamorphic Complex


## Summary

The dome-shaped Mount Schaber, located to the south of the Harts Range, which was initially mapped as a granite pluton, is shown to be a quartz and plagioclase-rich, hypersthene-bearing, felsic granofels. The granofels is conformable with other felsic and mafic gneisses in the Strangways Metamorphic Complex, and folded into a doubly plunging antiform (*sheath fold*). The Mount Schaber granofels and adjacent felsic gneisses are unusually depleted in K, Rb, and REE compared to other Australian Proterozoic felsic rocks, and are compositionally unlike many unaltered igneous rocks. The K-poor composition of the Mount Schaber felsic rocks is analogous with rhyolitic tephras in the Permian Newcastle Coal Measures (New South Wales, Australia) that have been altered to a fine-grained assemblage of quartz, analcime and calcite or quartz-adularia. The Mount Schaber felsic rocks may have formed from the metamorphosed equivalents of similarly altered tephras. In more retrogressed samples, Cl-rich magnesio-hastingsite rims hypersthene, and scapolite occurs along plagioclase grain boundaries, owing to probable fluid movement after the granulite facies metamorphic peak ($M_1$). A high Cl activity during hydrous retrogression may have been responsible for local movement of the 'immobile' element Y, which is strongly depleted in the more recrystallized, retrogressed samples. Contrasting rheological properties and fluid movement, causing strain softening may have also been significant in producing the sheath-like fold structure during a major regional non-coaxial deformation[1].


[1] Norman, A. R. and Flood, R. H., 1991. Geochemistry and structure of a K-poor granofels: a possible quartz-analcime altered tephra? Mount Schaber, central Australia. *Journal of Metamorphic Geology* (accepted).

## 1.1 Introduction

Mount Schaber is situated to the east of Cattlewater Pass, south of the Harts Range, central Australia (Fig. 1.1), and has a distinctive dome-like outcrop that led Joklik (1955) to believe that it was a granite intruded into the surrounding Cadney Gneiss. The pluton was named the Schaber hornblende-granite and the modal data provided were of a quartz-rich hornblende leucogranite containing 37.5% microperthitic microcline and apparently no hypersthene. The most recent map of the area (1:100,000 Arltunga-Harts Range Region; Shaw et al., 1984b) shows Mount Schaber as either a granite or a felsic granulite, suggesting that the authors saw at least some evidence for this body not being a granite. The rocks at Mount Schaber form the eastern margin of the early-Proterozoic Ongeva granulites, which belong to the Strangways Metamorphic Complex (Shaw et al., 1984a) and have been interpreted as a bimodal suite of extrusives and shallow intrusives (Shaw et al., 1979; Shaw et al., 1984a, 1984b; Shaw and Langworthy, 1984; Warren and Shaw, 1985). In this study, field mapping (Fig. 1.2) showed that Mount Schaber consists of a massive granofels concordant with other gneisses. An examination of geochemical and petrographic data also indicated that the Mount Schaber granofels and adjacent felsic gneisses are unlike many Proterozoic and unaltered Phanerozoic granites. In this Chapter, the felsic rocks at Mount Schaber are interpreted as having been altered rhyolitic tephras, which were deformed into a *sheath-like* antiform during a major tectonometamorphic event.

## 1.2 Petrology

The variation in bulk rock composition throughout the Ongeva granulites, including the Mount Schaber area, is defined by cm to m-scale layers. These compositional layers may reflect a primary sedimentary layering, although they have been commonly boudinaged due to deformation. The gross compositional boundaries are here referred to as $S_1$ because they have commonly been modified by deformation and because no evidence for primary bedding or layering has been recognized. The

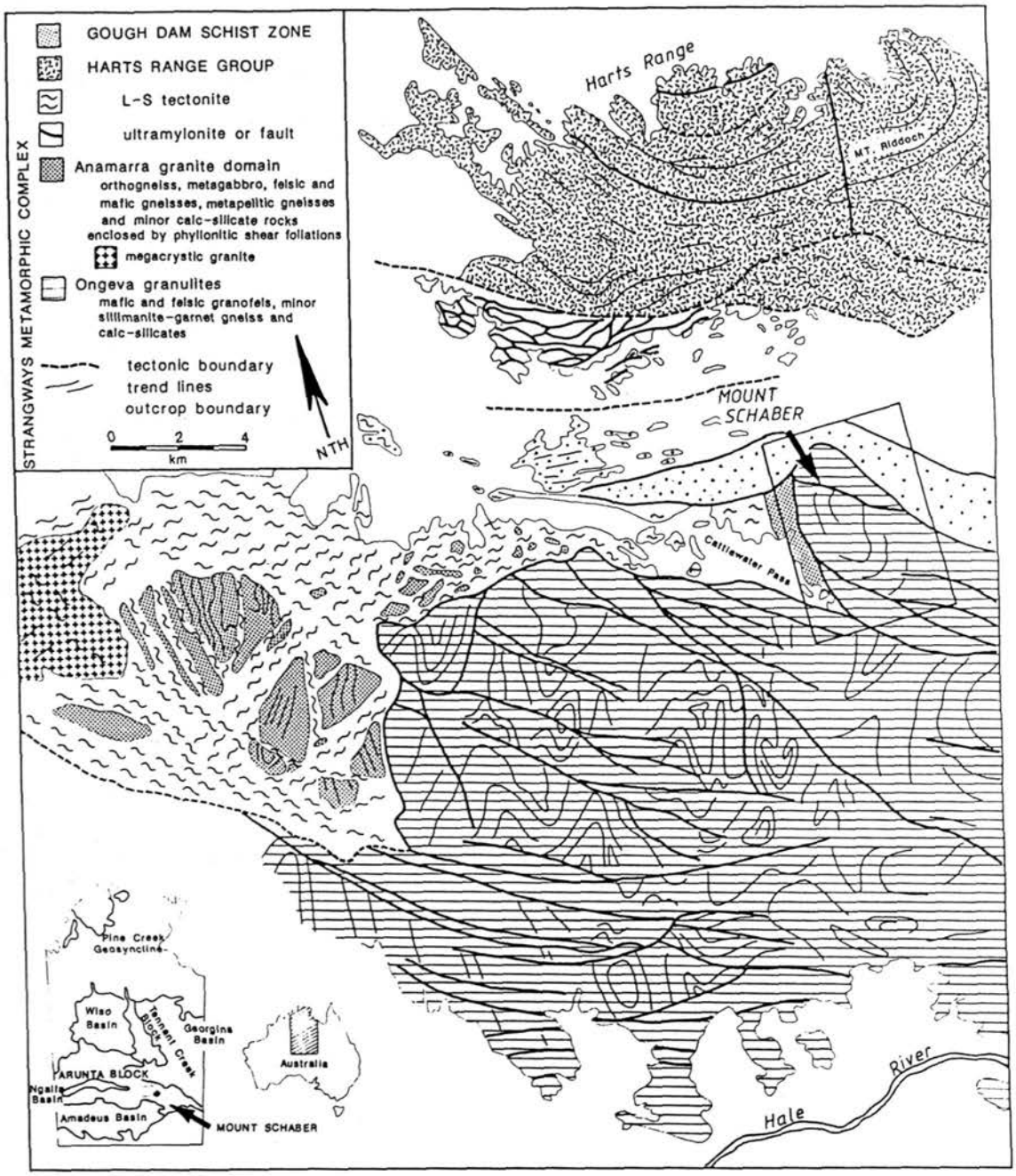


**Fig. 1-1** Geological map of an area south of the Harts Range showing the Ongeva granulites, Anamarra granite domain and Harts Range Group.

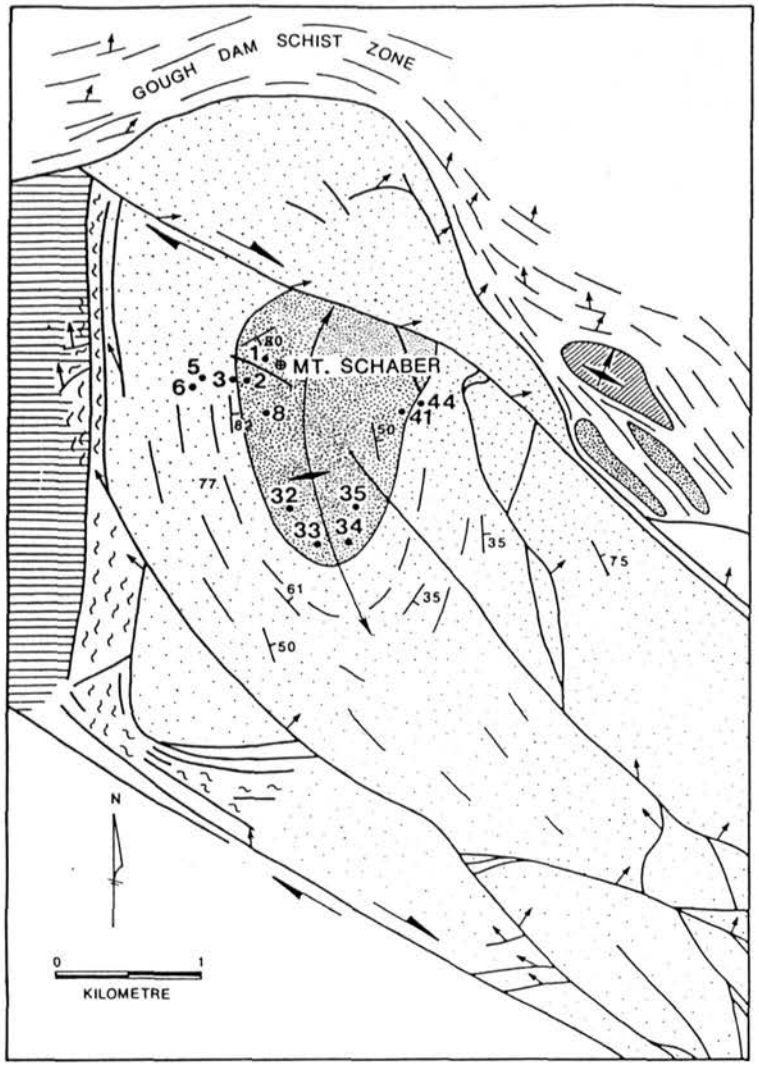


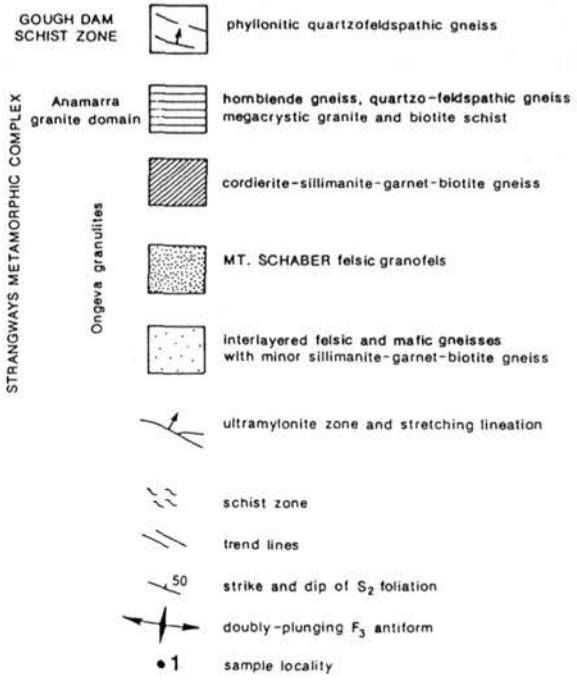


**Fig. 1-2** Geology of the Mount Schaber area.

interlayered felsic and mafic gneisses around Mount Schaber also contain a tectonometamorphic gneissic foliation ($S_2$) that is defined by coarse-grained leucosome layers (Fig. 1.3a), which probably crystallized from partial melt. $S_2$ is generally sub-parallel to $S_1$ compositional boundaries and forms an axial plane foliation to isoclinal, rootless, intrafolial $F_2$ folds. The widespread granulite facies metamorphism in the Strangways Metamorphic Complex, which has been dated at about 1800 Ma (Iyer et al., 1976; Black et al., 1983; Windrim and McCulloch, 1986) is probably equivalent to the earliest metamorphic event ($M_1$) recognized in the Mount Schaber rocks. Recrystallization, grainsize reduction and retrogression preserved in the Mount Schaber granofels may also represent the effects of a second granulite facies metamorphism ($M_2$) recognized elsewhere by Iyer et al. (1976) and Norman and Clarke (1990). The structural and metamorphic evolution of the Strangways Metamorphic Complex is discussed in more detail in the following Chapters.

In this Chapter, the unusual geochemical composition of a felsic granofels and adjacent felsic gneisses in the Ongeva granulites is described. The composition of this unusual granofels and other felsic, mafic and metapelitic gneisses in the Ongeva granulites, which are also briefly described, may indicate the nature of the precursors to high-grade gneisses in the Strangways Metamorphic Complex. The use of geochemistry may also help to delineate the tectonic setting in which high-grade gneisses were formed. However, metamorphism, deformation and fluid movement may have extensively modified the composition of the rocks. Therefore, it is essential in any high-grade terrain that the effects of the tectonometamorphic history be recognized and removed in order to interpret the possible precursors. In this Chapter, diagenetic alteration and fluid movement after peak metamorphism are interpreted to have changed the precursor composition of felsic rocks at Mount Schaber, which is unlike the composition of other felsic rocks in the Strangways Metamorphic Complex, other felsic Proterozoic rocks and unaltered Phanerozoic igneous rocks.

**Fig. 1-3 (a)** $S_2$ leucosome layers in a felsic gneiss adjacent to the Mount Schaber granofels.

**1.3 (b)** Outcrop of the Mount Schaber granofels.

**1.3 (c)** Magnesio-hastingsite hornblende rimming orthopyroxene. Base of photo is 4.4 mm.

**1.3 (d)** Scapolite filling pullaparts in andesine. Base of photo is 1.75 mm.

**1.3 (e)** Myrmekite and scapolite at a $M_1$ plagioclase grain boundary. Base of photo is 1.75 mm.

**1.3 (f)** $M_2$ scapolite and recrystallized andesine at a $M_1$ andesine grain boundary. Base of photo is 1.75 mm.

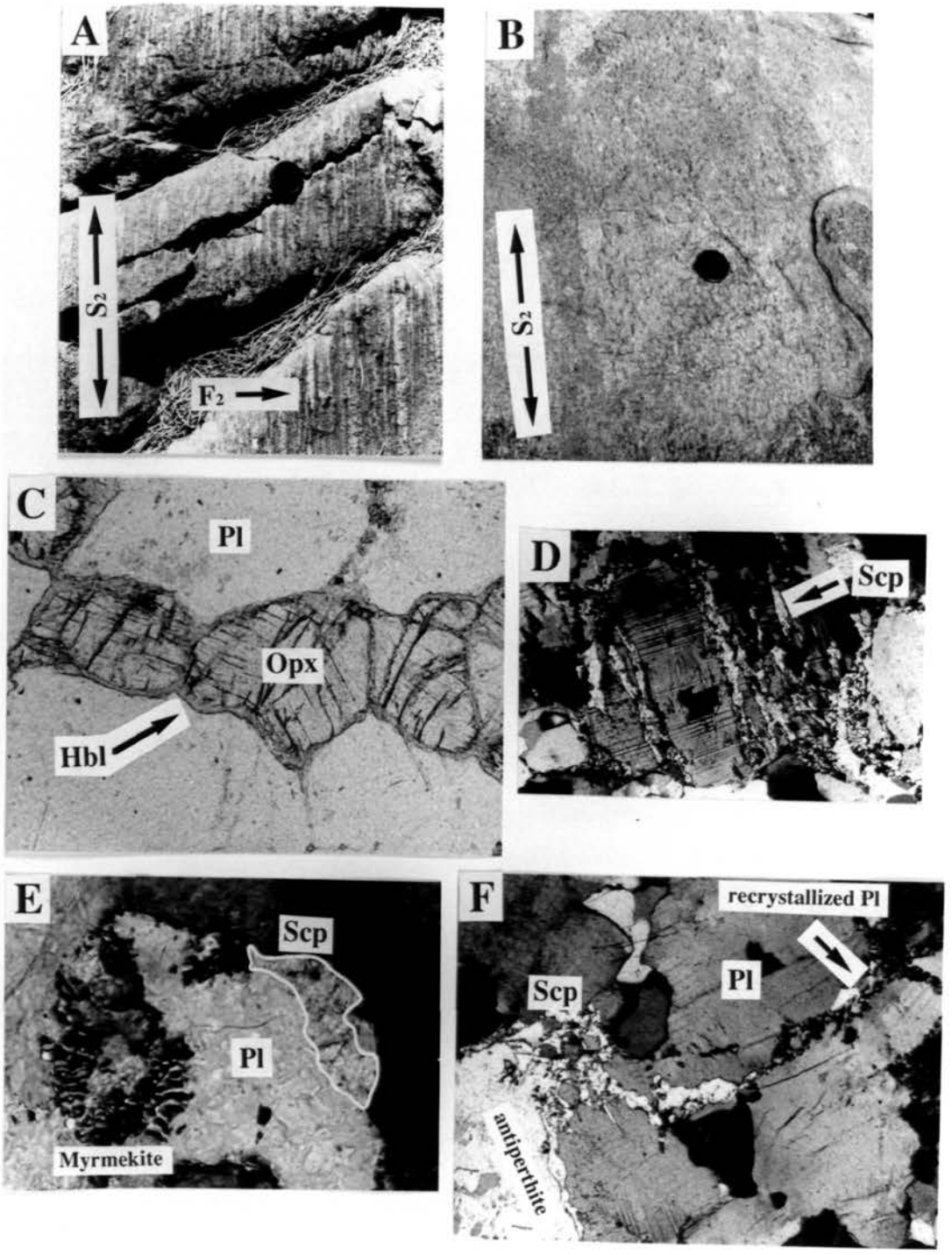
A
S2
F2
B
S2
C
Pl
Opx
Hbl
D
Scp
E
Scp
Pl
Myrmekite
F
recrystallized Pl
Scp
Pl
antiperthite

## 1.21 Petrography

*Mount Schaber granofels:* The Mount Schaber granofels is a folded, massive unit within the Ongeva granulites, but is distinguished from other felsic rocks in the Ongeva granulites by its unusual, K-poor chemistry and relative depletion in Rb and REE. The granofels is pale grey in colour and as noted by Joklik (1955) has a pronounced joint structure. It is generally of an even grainsize with a granoblastic texture, but has only a weakly developed $S_2$ foliation defined by leucocratic layering and/or biotite (Fig. 1.3b). In thin section, the rock is seen to be composed largely of andesine, antiperthitic andesine and quartz, with a small percentage of hypersthene and opaque minerals. Representative microprobe analyses are shown in Table 1.1 The least deformed samples consist of polygonal quartz with large equant grains of antiperthite and smaller equant hypersthene grains that occur at the triple junctions of the larger grains of quartz and feldspar. The assemblage hypersthene-plagioclase-quartz±K-feldspar represents the effects of peak metamorphism ($M_1$) in the Mount Schaber granofels.

In all samples of the Mount Schaber granofels, the coarse-grained $M_1$ minerals have been deformed, partly recrystallized and, in places, retrogressed. These microstructures appear to represent the effects of a second metamorphism ($M_2$). Coarse-grained quartz is commonly elongate, with undulose extinction and recrystallized quartz grains that have a preferred crystallographic orientation oblique to $S_2$. $M_1$ plagioclase usually shows significant recrystallization and grain-size reduction around grain boundaries. In the more deformed samples, $M_1$ hypersthene is partly or totally replaced by steel-blue magnesio-hastingsite (Fig. 1.3c) and $M_1$ plagioclase has deformation twins and shows brittle deformation in the form of pull-aparts Fig. (Fig. 1.3d) that are filled with fine-grained scapolite ($X_{An}$ = 0.35-0.40). Scapolite also occurs with fine-grained recrystallized plagioclase aggregates and myrmekite along some $M_1$ plagioclase grain boundaries (Figs 1.3e, 1.3f), possibly replacing plagioclase. Myrmekite is rare in the less deformed, coarse-grained granofels samples. Biotite is also

**Table 1.1** Representative micrprobe analyses of minerals in sample 2, Mount Schaber granofels.*

| wt% | Opx | Hbl | Bt | Pl | antiperthite Kfs | antiperthite andesine | Pl M2 | scapolite |
|---|---|---|---|---|---|---|---|---|
| $SiO_2$ | 51.11 | 35.16 | 34.81 | 60.59 | 64.06 | 60.94 | 59.76 | 57.38 |
| $TiO_2$ | - | 0.27 | 4.38 | - | - | - | - | - |
| $Al_2O_3$ | 1.17 | 15.01 | 14.28 | 25.00 | 20.15 | 24.52 | 25.55 | 24.04 |
| $Cr_2O_3$ | - | - | - | - | - | - | - | - |
| FeO | 30.33 | 24.68 | 24.19 | - | - | - | - | - |
| MnO | 0.34 | - | - | - | - | - | - | - |
| MgO | 17.14 | 4.32 | 8.03 | 0.28 | 0.40 | 0.29 | 0.24 | - |
| CaO | 0.13 | 10.00 | | 6.62 | 1.42 | 6.10 | 6.74 | 7.26 |
| $Na_2O$ | - | 0.87 | 0.39 | 7.67 | 1.97 | 7.10 | 7.48 | 8.10 |
| $K_2O$ | - | 3.22 | 8.78 | 0.37 | 12.46 | 1.58 | 0.19 | 0.63 |
| Cl | - | 4.96 | 2.60 | - | - | - | - | 1.46 |
| TOTAL | 100.22 | 98.49 | 97.46 | 100.53 | 100.44 | 100.53 | 99.96 | 98.87 |
| structural analysis | | | | | | | | |
| basis of | 6 (O) | 23 (O) | 22 (O) | 32 (O) | 32 (O) | 32 (O) | 32 (O) | 32 (O) |
| Si | 1.97 | 5.69 | 5.59 | 10.74 | 11.67 | 10.83 | 10.65 | 10.42 |
| Ti | - | 0.04 | 0.53 | - | - | - | - | |
| $Al^{IV}$ | 0.03 | 2.31 | 2.41 | 5.22 | 4.32 | 5.14 | 5.37 | 5.15 |
| $Al^{VI}$ | 0.02 | 0.55 | 0.30 | - | - | - | - | - |
| Cr | - | - | - | - | - | - | - | - |
| $Fe^{2+}$ | 0.97 | 0.34 | 3.25 | - | - | - | - | - |
| $Fe^{3+}$ | 0.01 | 3.00 | - | - | - | - | - | - |
| Mn | 0.01 | - | - | - | - | - | - | - |
| Mg | 0.98 | 1.04 | 1.92 | 0.07 | 0.11 | 0.08 | 0.06 | - |
| Ca | 0.01 | 1.73 | - | 1.26 | 0.28 | 1.16 | 1.29 | 1.41 |
| Na | - | 0.27 | 0.12 | 2.63 | 0.70 | 2.45 | 2.58 | 2.85 |
| K | - | 0.67 | 1.80 | 0.08 | 2.89 | 0.36 | 0.04 | 0.15 |
| TOTAL | 4.01 | 15.97 | 15.92 | 20.00 | 19.96 | 19.99 | 20.01 | 20.43 |

* mineral compositions were analysed at Macquarie University using a wave-length dispersive system on a ETEC microprobe at 15KV and specimen current of 50nA.

more abundant in the more deformed samples, occurring with magnesio-hastingsitic hornblende and as clots around opaque minerals.

*Felsic gneisses*: Felsic gneisses interlayered with mafic granofelses adjacent to the Mount Schaber granofels have assemblages and microstructures similar to those in the Mount Schaber granofels. Like the Mount Schaber granofels, some of the adjacent felsic gneisses are largely composed of plagioclase. However, the composition of the Mount Schaber granofels and plagioclase-rich gneisses is unlike most felsic gneisses in the Ongeva granulites, which are generally richer in orthoclase and perthite. This Chapter aims to interpret the unusual geochemistry of these K-feldspar-poor felsic rocks to determine whether the different composition is related to the original source rock composition or due to metamorphic and/or deformation processes.

*Mafic granofelses:* Mafic granofelses are interlayered with felsic gneisses around the margin of Mount Schaber and also occur as minor mesoscopic and microscopic enclaves in the Mount Schaber granofels. A granoblastic orthopyroxene-clinopyroxene-plagioclase±hornblende±quartz assemblage represents $M_1$. The effects of $M_2$ are recognized by recrystallization around grain boundaries, minor rims of pargasitic hornblende on orthopyroxene, fine-grained symplectic intergrowths of orthopyroxene-plagioclase±clinopyroxene±hornblende at the interface between $M_1$ plagioclase and hornblende, and fine-grained plagioclase-clinopyroxene symplectites at the interface between $M_1$ clinopyroxene and hornblende (Chapters 3 and 4). The small (1.5 cm long) mafic enclaves in the Mount Schaber granofels also contain $M_2$ symplectites and microstructures.

*Metapelites:* Minor metapelitic gneisses are interlayered with quartzofeldspathic gneisses and mafic granofelses that surround the Mount Schaber granofels. An $S_1$ tectonometamorphic foliation is commonly preserved as folded inclusions of fine-grained sillimanite and spinel-ilmenite in garnet and cordierite porphyroblasts. Spinel and quartz inclusions also occur in cordierite. A peak metamorphic ($M_1$) assemblage in metapelites probably included spinel and quartz with K-feldspar-sillimanite-

ilmenite±garnet±cordierite. A coarse-grained sillimanite-biotite-magnetite $S_{2b}$ foliation commonly anastomoses through the $S_2$ leucosome foliation. In cordierite-rich gneisses, coarse-grained cordierite is partly replaced by a hypersthene-sillimanite-quartz±magnetite±biotite symplectite. This symplectite also envelops the coarse-grained $S_{2b}$ sillimanite and represents a second metamorphic paragenesis, which is discussed in Chapter 3 ($M_2$, Norman and Clarke, 1990).

*Ultramylonites:* Narrow shear zones containing ultramylonite cut $S_1$, $S_2$, and the folded Mount Schaber granofels. Ultramylonitized felsic granofelses commonly contain recrystallized hypersthene and andesine porphyroclasts, which have recrystallized tails of more sodic plagioclase and, in places, scapolite. Myrmekite is common in felsic granofelses and gneisses, adjacent to the shear zones. In ultramylonitized garnet-bearing gneisses, garnet is recrystallized or is partially replaced by biotite. In ultramylonitized mafic granofelses, orthopyroxene and clinopyroxene are recrystallized and the recrystallized pyroxene composition is commonly similar to the composition of $M_2$ pyroxenes (Chapter 5; Norman and Vernon, 1991).

## 1.22 Geochemistry of the Mount Schaber granofels and adjacent felsic gneisses

Outcrop mapping shows that the Mount Schaber granofels is conformable with the surrounding gneisses and is not a discordant pluton (Fig. 1.2). Its thickness is probably greater than 100m. Analyses of the Mount Schaber granofels and adjacent felsic gneisses are presented in Table 1.2 and sample localities are shown on Fig. 1.2. Average analyses of felsic, mafic and meta pelitic gneisses elsewhere from the Ongeva granulites are presented in Table 1.3. The most conspicuous feature of the granofels and adjacent felsic gneisses is their low $K_2O$ content. All samples except samples 41 and 44, which occur on the margin of the granofels, are poor in normative orthoclase (Fig. 1.4). $K_2O$ is less than 1.51 wt% except in these two samples. All samples are rich in normative quartz and plagioclase (An+Ab). $SiO_2$ is everywhere greater than 73 wt %. The ratio of $Al_2O_3/(Na_2O+K_2O+CaO)$ is less than 1.1 and most samples have no or little

**Table 1.2** Major and trace element analyses of the Mount Schaber granofels and adjacent felsic gneisses (localities on Fig. 1-2).

| | Mount Schaber granofels | | | | | | | | | felsic gneisses adjacent to the Mount Schaber granofels | | | | |
|---|---|---|---|---|---|---|---|---|---|---|---|---|---|---|
| wt% | 1 | 2 | 8 | 32 | 33 | 34 | 35 | 35B | 41 | 3 | 5 | 5B | 6 | 44 |
| $SiO_2$ | 78.09 | 76.1 | 74.55 | 73.67 | 77.13 | 76.95 | 79.69 | 78.83 | 75.34 | 75.92 | 78.15 | 77.83 | 75.74 | 74.15 |
| $TiO_2$ | 0.29 | 0.21 | 0.68 | 0.54 | 0.28 | 0.28 | 0.1 | 0.17 | 0.25 | 0.43 | 0.36 | 0.09 | 0.48 | 0.35 |
| $Al_2O_3$ | 12.77 | 13.25 | 12.89 | 12.77 | 13.1 | 12.56 | 12.05 | 11.62 | 11.73 | 12.75 | 12.40 | 12.89 | 12.99 | 11.54 |
| $Fe_2O_3$ | 0.30 | 0.30 | 0.65 | 1.20 | 0.32 | 0.41 | 0.15 | 0.37 | 1.58 | 0.55 | 0.23 | 0.34 | 0.44 | 1.11 |
| FeO | 0.48 | 1.00 | 1.69 | 2.23 | 0.52 | 1.10 | 0.25 | 0.56 | 1.43 | 1.28 | 0.73 | 0.29 | 1.29 | 2.44 |
| MnO | 0.02 | 0.01 | 0.03 | 0.03 | 0.02 | 0.02 | 0.00 | 0.00 | 0.03 | 0.01 | 0.01 | 0.01 | 0.03 | 0.04 |
| MgO | 0.23 | 0.39 | 0.67 | 0.85 | 0.11 | 0.45 | 0.03 | 0.34 | 0.27 | 0.60 | 0.19 | 0.25 | 0.49 | 1.32 |
| CaO | 3.28 | 3.31 | 3.68 | 3.48 | 3.17 | 3.25 | 2.69 | 3.13 | 1.67 | 3.19 | 2.89 | 3.46 | 3.88 | 0.79 |
| $Na_2O$ | 3.55 | 3.89 | 3.84 | 3.40 | 3.73 | 3.78 | 4.04 | 3.74 | 2.54 | 3.50 | 3.77 | 3.49 | 3.71 | 2.21 |
| $K_2O$ | 0.73 | 1.11 | 0.66 | 1.51 | 1.1 | 0.75 | 0.57 | 0.39 | 4.48 | 1.12 | 0.79 | 0.77 | 0.67 | 5.62 |
| $P_2O_4$ | 0.01 | 0.01 | 0.14 | 0.07 | 0.01 | 0.01 | 0.00 | 0.00 | 0.04 | 0.00 | 0.00 | 0.00 | 0.00 | 0.04 |
| $H_2O+$ | 0.21 | 0.23 | 0.29 | 0.22 | 0.23 | 0.24 | 0.21 | 0.24 | 0.25 | 0.34 | 0.27 | 0.23 | 0.24 | 0.25 |
| $H_2O-$ | 0.06 | 0.07 | 0.06 | 0.04 | 0.05 | 0.06 | 0.07 | 0.02 | 0.07 | 0.04 | 0.04 | 0.12 | 0.10 | 0.05 |
| $CO_2$ | 0.07 | 0.08 | 0.07 | 0.01 | 0.10 | 0.08 | 0.02 | 0.05 | 0.02 | 0.07 | 0.06 | 0.12 | 0.08 | 0.03 |
| TOTAL | 100.09 | 99.96 | 99.9 | 100.02 | 99.87 | 99.94 | 99.87 | 99.46 | 99.70 | 99.8 | 99.88 | 99.89 | 100.14 | 99.95 |
| S.I Index | 1.01 | 0.97 | 0.94 | 0.94 | 1.00 | 0.97 | 0.99 | 0.95 | 0.97 | 1.00 | 1.01 | 1.00 | 0.94 | 1.03 |
| trace elements (ppm) | | | | | | | | | | | | | | |
| Ba | 122 | 297 | 96 | 304 | 194 | 86 | 77 | 45 | 815 | 174 | 115 | 108 | 90 | 1120 |
| Ce | 35 | 27 | 22 | 43 | 38 | 27 | 24 | 21 | 98 | 18 | 21 | 30 | 19 | 88 |
| Cr | 6 | 4 | 3 | 4 | 7 | 6 | 4 | 2 | 3 | 4 | 8 | 6 | 5 | 4 |
| Cu | 15 | 16 | 17 | 20 | 16 | 13 | 16 | 10 | 17 | 13 | 14 | 12 | 12 | 23 |
| Ga | 18 | 18 | 21 | 20 | 19 | 17 | 21 | 19 | 21 | 16 | 14 | 15 | 17 | 17 |
| La | 9 | 9 | 0 | 15 | 9 | 5 | 0 | 0 | 42 | 0 | 0 | 11 | 6 | 47 |
| Nb | 9 | 4 | 19 | 13 | 10 | 11 | 3 | 9 | 15 | 9 | 4 | 1 | 11 | 19 |
| Nd | 10 | 11 | 14 | 28 | 18 | 19 | 12 | 10 | 52 | 10 | 19 | 17 | 15 | 41 |
| Ni | 1 | 2 | 5 | 8 | 2 | 1 | 1 | 2 | 6 | 5 | 1 | 1 | 2 | 9 |
| Pb | 2 | 3 | 7 | 4 | 3 | 9 | 4 | 4 | 6 | 6 | 4 | 11 | 4 | 12 |
| Pr | 0 | 0 | 0 | 0 | 0 | 0 | 0 | 0 | 14 | 0 | 0 | 0 | 0 | 12 |
| Rb | 8 | 19 | 6 | 25 | 20 | 14 | 11 | 7 | 130 | 28 | 13 | 8 | 14 | 201 |
| Sr | 144 | 143 | 119 | 108 | 124 | 119 | 122 | 122 | 89 | 120 | 127 | 110 | 128 | 56 |
| Th | 4 | 0 | 41 | 0 | 1 | 42 | 42 | 35 | 36 | 12 | 20 | 3 | 6 | 31 |
| U | 1 | 0 | 3 | 2 | 2 | 2 | 2 | 2 | 3 | 1 | 1 | 2 | 1 | 6 |
| V | 11 | 16 | 46 | 42 | 11 | 11 | 12 | 10 | 11 | 19 | 17 | 8 | 66 | 7 |
| Y | 2 | 4 | 26 | 34 | 2 | 22 | 3 | 11 | 92 | 2 | 1 | 0 | 2 | 61 |
| Zn | 5 | 10 | 10 | 16 | 7 | 11 | 4 | 6 | 19 | 12 | 9 | 7 | 13 | 37 |
| Zr | 306 | 255 | 386 | 370 | 352 | 285 | 226 | 280 | 289 | 409 | 301 | 295 | 504 | 382 |
| K/Rb | 913 | 584 | 1100 | 604 | 550 | 536 | 518 | 557 | 345 | 400 | 608 | 963 | 479 | 280 |
| CIPW norms | | | | | | | | | | | | | | |
| Qtz | 47.42 | 41.35 | 40.9 | 38.94 | 44.45 | 44.27 | 48.21 | 48.62 | 39.31 | 43.21 | 46.62 | 47.08 | 42.63 | 34.91 |
| Or | 4.29 | 6.55 | 3.89 | 8.93 | 6.48 | 4.41 | 3.39 | 2.29 | 26.47 | 6.60 | 4.66 | 4.53 | 3.93 | 33.20 |
| Ab | 30.05 | 32.87 | 32.51 | 28.78 | 31.58 | 31.96 | 34.17 | 31.68 | 21.45 | 29.62 | 31.93 | 29.64 | 31.4 | 18.72 |
| An | 15.79 | 15.43 | 15.96 | 15.10 | 15.05 | 15.10 | 13.04 | 13.75 | 7.40 | 15.36 | 13.95 | 16.41 | 16.82 | 3.49 |
| Crn | 0.35 | 0.00 | 0.00 | 0.00 | 0.25 | 0.00 | 0.00 | 0.00 | 0.00 | 0.15 | 0.22 | 0.30 | 0.00 | 0.54 |
| Di | 0 | 0.35 | 0.77 | 1.36 | 0.00 | 0.36 | 0.12 | 1.18 | 0.45 | 0.00 | 0.00 | 0.00 | 1.57 | 0.00 |
| Hy | 0.75 | 2.06 | 2.78 | 3.7 | 0.53 | 2.19 | 0.2 | 0.71 | 1.41 | 2.71 | 1.05 | 0.73 | 1.72 | 6.35 |
| Ol | 0.00 | 0.00 | 0.00 | 0.00 | 0.00 | 0.00 | 0.00 | 0.00 | 0.00 | 0.00 | 0.00 | 0.00 | 0.00 | 0.00 |
| Mag | 0.43 | 0.44 | 0.94 | 1.74 | 0.46 | 0.60 | 0.22 | 0.54 | 2.29 | 0.79 | 0.33 | 0.49 | 0.64 | 1.61 |
| Ilm | 0.56 | 0.40 | 1.29 | 1.03 | 0.54 | 0.53 | 0.00 | 0.00 | 0.47 | 0.81 | 0.68 | 0.18 | 0.91 | 0.67 |
| Ap | 0.02 | 0.02 | 0.34 | 0.16 | 0.02 | 0.02 | 0.19 | 0.33 | 0.09 | 0.01 | 0.00 | 0.00 | 0.01 | 0.09 |
| Cal | 0.16 | 0.18 | 0.16 | 0.02 | 0.23 | 0.18 | 0.05 | 0.11 | 0.05 | 0.16 | 0.14 | 0.27 | 0.18 | 0.07 |
| $H_2O$ | 0.27 | 0.30 | 0.35 | 0.26 | 0.28 | 0.30 | 0.28 | 0.26 | 0.32 | 0.38 | 0.31 | 0.35 | 0.34 | 0.30 |

**Table 1.3** Averaged analyses from the Ongeva granulites.*

| wt% | felsic gneiss | mafic granofels | metapelites |
|---|---|---|---|
| samples | 20 | 11 | 15 |
| $SiO_2$ | 73.20 | 50.43 | 52.69 |
| $TiO_2$ | 0.41 | 1.30 | 0.89 |
| $Al_2O_3$ | 12.84 | 14.79 | 23.71 |
| $Fe_2O_3$ | 1.33 | 3.22 | 5.67 |
| FeO | 1.39 | 8.21 | 5.43 |
| MnO | 0.02 | 0.13 | 0.13 |
| MgO | 0.52 | 7.24 | 3.31 |
| CaO | 1.31 | 10.57 | 0.83 |
| $Na_2O$ | 2.21 | 2.21 | 0.95 |
| $K_2O$ | 5.98 | 0.73 | 5.24 |
| $P_2O_4$ | 0.07 | 0.14 | 0.05 |
| $H_2O+$ | 0.32 | 0.55 | 0.82 |
| $H_2O-$ | 0.07 | 0.05 | 0.12 |
| $CO_2$ | 0.06 | 0.12 | 0.17 |
| TOTAL | 99.73 | 99.69 | 99.99 |
| trace elements (ppm) | | | |
| Ba | 1008 | 115 | 858 |
| Ce | 66 | 46 | 93 |
| Cr | 7 | 254 | 163 |
| Cu | 20 | 52 | 15 |
| Ga | 15 | 19 | 36 |
| La | 33 | 19 | 57 |
| Nb | 10 | 11 | 14 |
| Nd | 30 | 26 | 35 |
| Ni | 9 | 78 | 58 |
| Pb | 12 | 7 | 21 |
| Pr | 7 | 7 | 14 |
| Rb | 219 | 25 | 220 |
| Sr | 89 | 104 | 83 |
| Th | 21 | 2 | 26 |
| U | 2 | 2 | 1 |
| V | 18 | 244 | 133 |
| Y | 19 | 73 | 31 |
| Zn | 15 | 83 | 125 |
| Zr | 262 | 99 | 185 |

* analyses of felsic, mafic and metapelitic gneisses from the Ongeva granulites are given in the appendix to this chapter

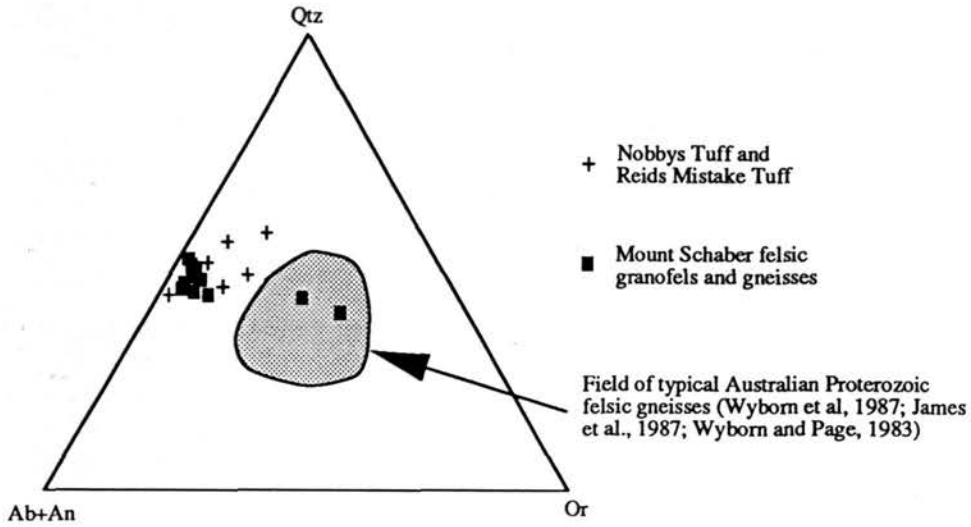


**Fig. 1.4** Ternary plot of normative quartz, plagioclase (An+Ab) and orthoclase for the Mount Schaber granofels and adjacent felsic gneisses.

normative corundum. The chemical variation of the Mount Schaber granofels and adjacent felsic gneisses is shown on selected Harker diagrams (Fig. 1.5a). $TiO_2$, MgO, $K_2O$ and CaO tend to decrease linearly with increasing $SiO_2$ content. A plot of $Na_2O+K_2O$ against $Na_2O/K_2O$ (Fig. 1.5b) indicates an enrichment of Na relative to K. Zr and Ga show a linear relationship with $SiO_2$, but there appears to be no relationship between Y and $SiO_2$ content. All samples, except 44, are depleted in Ba, La and Rb, compared with other felsic gneisses in the Ongeva granulites and typical felsic gneisses from Australian Proterozoic blocks (e.g. Wyborn et al., 1987; Wyborn, 1988). The Mount Schaber granofels and felsic gneisses have variable but higher K/Rb ratios compared with other felsic gneisses in the Ongeva granulites (Table 1.3) and also tend to be higher in CaO, $Na_2O$, Sr and Ga.

In an attempt to assess the primary rock types and affinities, individual elemental (or oxide) abundances have been plotted against ratios of assumed 'immobile' elements (Winchester and Floyd, 1977). A plot of Nb/Y against $Zr/TiO_2$ shows that Y-poor samples fall in the trachyte and trachyandesite fields, whereas a plot of $SiO_2$ against $Zr/TiO_2$ (Fig. 1.5c) shows a linear variation between rhyodacite and rhyolitic compositions. The apparent conflict between these plots may be attributed to a variable depletion of Y (see discussion). Covariance plots show that Zr, Ga (Fig. 1.5d) and Nb increase linearly with $TiO_2$ and this may reflect original rock composition produced by fractional crystallization of a common source. However, Y shows no correlation with Zr or $TiO_2$.

### 1.23 Altered rhyolitic tephras as a precursor?

Two undeformed tephra units in the Permian Newcastle Coal Measures of the Sydney Basin, New South Wales, Australia, show some chemical similarities with the Mount Schaber granofels and adjacent felsic gneisses by being poor in normative orthoclase and rich in plagioclase. These tephras outcrop along the coast, about 150 km north of Sydney, at Nobbys Head and Swansea Heads, and form two of the thickest tephra units of the Newcastle Coal Measures. They are called the *Nobbys Tuff* and the *Reids*

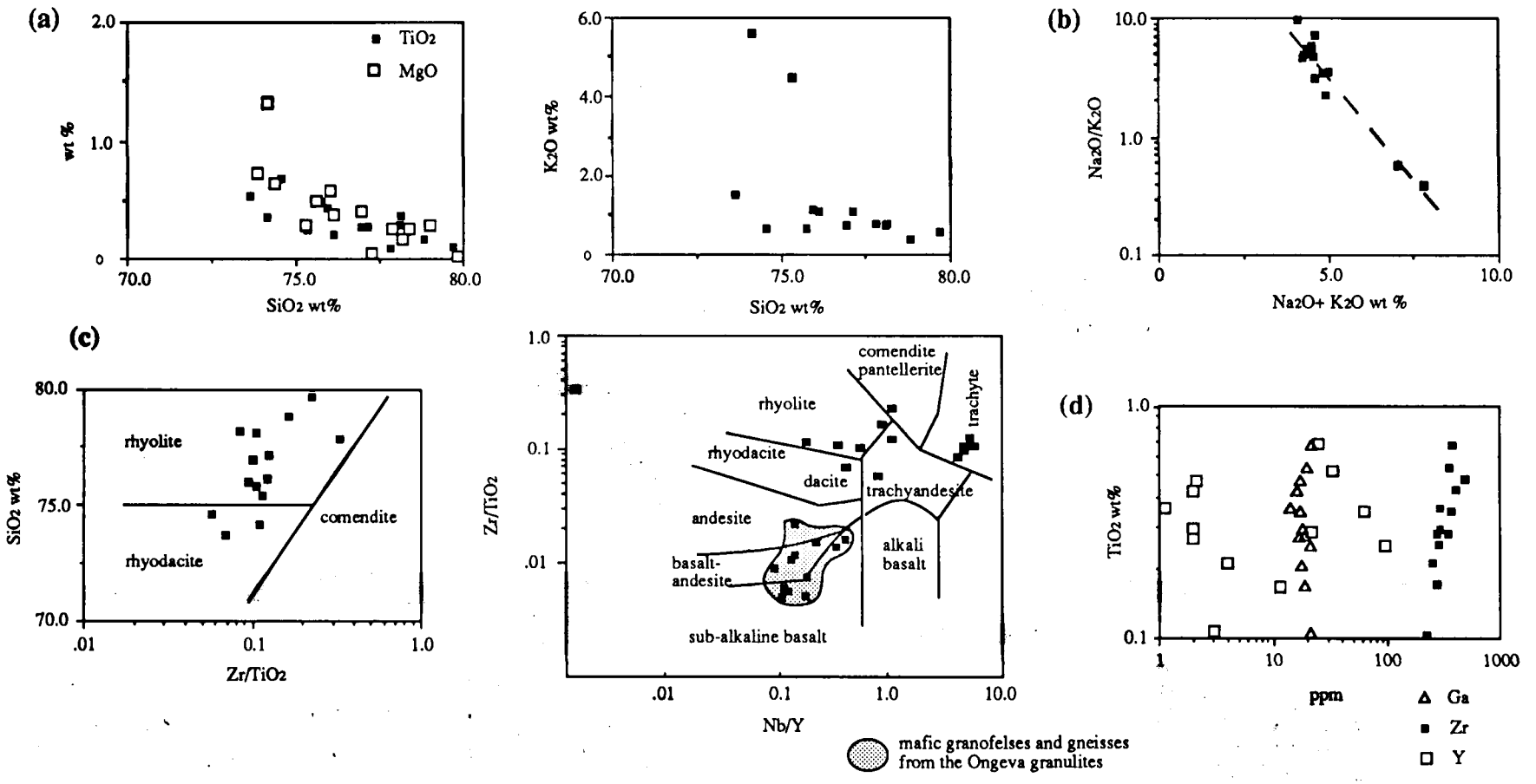


**Fig. 1.5** **(a)** Selected Harker diagrams for the Mount Schaber granofels and adjacent felsic gneisses.

**1.5 (b)** Plot of $Na_2O+K_2O$ against $Na_2O/K_2O$, Mount Schaber granofels and adjacent felsic gneisses.

**1.5 (c)** $SiO_2$ against $Zr/TiO_2$ discrimination diagram and $Zr/TiO_2$ against Nb/Y discrimination diagram for the Mount Schaber granofels and felsic gneisses and mafic rocks from the Ongeva granulites.

**1.5 (d)** Selected covariance diagrams for the Mount Schaber granofels and adjacent felsic gneisses.

*Mistake Tuff*, respectively (Diessel, 1980a). They are both fine to coarse-grained, vitric and clast-rich, and have bedding characteristics similar to those of a pyroclastic surge deposit (Mushenko, 1985). However, they probably also include airfall tephras and some reworked ash. The phenocrysts in both Tuffs are quartz, feldspar and (altered) biotite, an assemblage typical of subalkaline dacitic to rhyolitic rocks (Ewart, 1979). Outlines of glass shards are evident in both Tuffs (Diessel, 1980b; Mushenko, 1985). The glass has devitrified to chalcedony and analcime in the Reids Mistake Tuff (Loughnan and Ray, 1979) and to quartz and K-feldspar (? adularia) in the Nobbys Tuff (Mushenko, 1985).

Analyses of the Newcastle tephras from Mushenko (1985) are shown in Table 1.4. The Reids Mistake Tuff is generally richer in Na which Mushenko (1985) and Loughnan and Ray (1979) interpreted to reflect the presence of analcime and the Nobbys Tuff is richer in K, possibly reflecting quartz-adularia alteration (Mushenko 1985). Similarly, the K-poor Mount Schaber granofels and adjacent felsic gneisses may have been altered, vitric, felsic tephras and the variable K and Na content may reflect different alteration products in the precursors (e.g. analcimized or quartz-adularia).

## 1.3 Structure

The main structural elements of the Mount Schaber area are presented in Fig. 1.6. Around the margins of Mount Schaber, two-pyroxene mafic granofelses, garnet-bearing felsic gneisses and metapelitic gneisses are interlayered with hypersthene-bearing quartzofeldspathic gneisses and appear conformable with the Mount Schaber granofels. They contain a well-developed gneissosity ($S_2$) defined by mm to cm-scale leucosome layers, which is generally sub-parallel to $S_1$ compositional boundaries. In metapelitic gneisses, a coarse-grained, sillimanite-biotite-magnetite±corundum foliation ($S_{2b}$) anastomoses through the main, penetrative, $S_2$ leucocratic layering but is generally parallel to $S_2$. $S_1$ and $S_2$ are folded by colinear, inclined $F_3$ and $F_4$ folds. $F_3$ folds are tight to isoclinal, discontinuous, intrafolial and may have an axial planar quartz-rich mylonitic foliation. Medium to coarse-grained biotite may also be aligned in $S_3$ and pods

**Table 1.4** Major and trace element analyses of the Reids Mistake Tuff and the Nobbys Tuff, Newcastle Coal Measures, Sydney Basin.

| | Reids Mistake Tuff | | Nobbys Tuff | | | |
|---|---|---|---|---|---|---|
| wt% | S8 | S9 | N2A | N2B | N2CC | N2DC |
| $SiO_2$ | 79.21 | 77.58 | 66.73 | 63.79 | 69.39 | 73.77 |
| $TiO_2$ | 0.12 | 0.12 | 0.5 | 0.54 | 0.45 | 0.58 |
| $Al_2O_3$ | 11.31 | 12.26 | 19.44 | 20.38 | 18.21 | 12.92 |
| $Fe_2O_3$ | 0.16 | 0.41 | 0.52 | 0.27 | 0.4 | 0.28 |
| FeO | 0.07 | 0.12 | 1.13 | 1.17 | 0.88 | 1.19 |
| MnO | 0.01 | 0.1 | 0 | 0 | 0 | 0 |
| MgO | 0.09 | 0.31 | 1 | 1 | 0.76 | 0.86 |
| CaO | 0.24 | 0.19 | 1.66 | 2.13 | 1.16 | 2.67 |
| $Na_2O$ | 5.85 | 4.7 | 2.77 | 2.92 | 2.23 | 2.54 |
| $K_2O$ | 0.3 | 0.94 | 2.02 | 1.53 | 1.92 | 1.15 |
| $P_2O_4$ | 0.01 | 0.01 | 0.12 | 0.12 | 0.11 | 0.18 |
| $H_2O+$ | 4.32 | 4.68 | 3.39 | 4.13 | 3.59 | 2.27 |
| $H_2O-$ | 0.51 | 0.19 | 0.46 | 0.43 | 0.55 | 0.36 |
| $CO_2$ | 0.14 | 0.15 | 0.37 | 0.99 | 0.09 | 1.77 |
| TOTAL | 102.34 | 101.76 | 100.11 | 99.4 | 99.74 | 100.54 |
| trace elements (ppm) | | | | | | |
| Ba | 297 | 605 | 764 | 697 | 391 | 533 |
| Ce | 0 | 0 | 116 | 39 | 141 | 122 |
| Cr | 3 | 35 | 28 | 264 | 162 | 284 |
| Cu | 29 | 34 | 8 | 38 | 66 | 47 |
| Ga | 22 | 18 | 23 | 23 | 19 | 21 |
| La | 0 | 0 | 65 | 15 | 80 | 67 |
| Nb | 3 | 2 | 8 | 21 | 3 | 8 |
| Ni | 11 | 26 | 16 | 111 | 51 | 114 |
| Pb | 14 | 10 | 17 | 14 | 5 | 11 |
| Rb | 21 | 16 | 113 | 46 | 25 | 50 |
| Sr | 680 | 887 | 502 | 677 | 762 | 608 |
| Th | 2 | 2 | 19 | 8 | 2 | 3 |
| U | 7 | 3 | 7 | 8 | 6 | 7 |
| V | 270 | 120 | 38 | 153 | 305 | 232 |
| Y | 21 | 6 | 13 | 15 | 16 | 19 |
| Zn | 181 | 62 | 73 | 98 | 85 | 95 |
| Zr | 72 | 56 | 164 | 216 | 70 | 11 |
| CIPW norms | | | | | | |
| Q | 43.43 | 45.82 | 37.82 | 34.77 | 45.53 | 47.66 |
| Or | 1.77 | 5.55 | 11.93 | 9.04 | 11.34 | 6.79 |
| Ab | 49.49 | 39.76 | 23.43 | 24.7 | 18.86 | 21.49 |
| An | 1.12 | 0.88 | 7.45 | 9.78 | 5.03 | 12.07 |
| C | 0.95 | 3.19 | 9.96 | 10.33 | 10.62 | 3.07 |
| Hy | 0.22 | 0.77 | 0 | 0 | 0 | 3.14 |
| Mt | 0 | 0.37 | 0 | 0 | 0 | 0.41 |
| Hm | 0.16 | 0.16 | 3.31 | 3.53 | 2.44 | 0 |
| Il | 0.17 | 0.23 | 0.75 | 0.39 | 0.58 | 1.1 |
| Ru | 0.03 | 0 | 0.95 | 1.03 | 0.85 | 0 |
| Ap | 0.02 | 0.02 | 0.28 | 0.28 | 0.26 | 0.43 |
| $H_2O$ | 4.83 | 4.87 | 3.85 | 4.56 | 4.14 | 2.63 |

**Table 1.5** Representative anaylses from Australian Proterozoic felsic gneisses and granites.

| | Arunta Block | | | Broken Hill Block | Mt Isa inlier |
|---|---|---|---|---|---|
| | Strangways Metamorphic Complex | | | | |
| wt% | (1) | (2) | (3) | (4) | (5) |
| $SiO_2$ | 76.72 | 76.50 | 71.52 | 73.1 | 73.27 |
| $TiO_2$ | 0.04 | 0.33 | 0.31 | 0.34 | 0.21 |
| $Al_2O_3$ | 13.13 | 11.20 | 14.24 | 14.21 | 13.63 |
| $Fe_2O_3$ | 0.49 | 1.51 | 0.33 | 2.22 | 0.42 |
| FeO | | 1.68 | 2.48 | | 1.41 |
| MnO | 0.05 | 0.35 | 0.06 | 0.01 | 0.03 |
| MgO | 0.01 | 0.25 | 0.68 | 0.54 | 0.38 |
| CaO | 0.66 | 1.31 | 2.52 | 1.23 | 1.67 |
| NaO | 3.58 | 2.51 | 3.02 | 2.07 | 2.69 |
| $K_2O$ | 5.36 | 4.39 | 3.35 | 6.17 | 5.07 |
| $P_2O_4$ | 0.01 | 0.02 | 0.1 | 0.09 | 0.06 |
| $H_2O+$ | | 0.08 | 0.57 | | |
| $H_2O-$ | 0.11 | 0.08 | | | |
| $CO_2$ | | 0.05 | 0.05 | | |
| TOTAL | 100.15 | 100.18 | 99.46 | 100.00 | 98.84 |
| trace elements (ppm) | | | | | |
| Ba | 119 | 840 | 660 | | 648 |
| Ce | 29 | | | | 104 |
| Cr | 6 | | | 13 | 8 |
| Cu | | | | | 6 |
| Ga | | | | | 15 |
| La | | | | | 57 |
| Nb | 27.8 | | | 9 | 9 |
| Nd | 12 | | | | 43 |
| Ni | 4 | | | 11 | 3 |
| Pb | | | | | 33 |
| Pr | | | | | |
| Rb | 125 | 175 | 260 | 259 | 227 |
| Sr | 34.2 | 46 | 85 | 43 | 159 |
| Th | | | | | 31 |
| U | | | | | 4 |
| V | 3 | | | 36 | 12 |
| Y | 22.5 | | | 9 | 24 |
| Zn | | | | | 28 |
| Zr | 59 | 460 | 210 | 135 | 143 |

(1) Inkamulla Granite Gneiss, Entia Dome, Foden et al. (1988)
(2) Quartzofeldspathic gneiss, Strangways Range, Warren and Shaw and (1985)
(3) Quartzofeldspathic gneiss, Edwards Creek, Warren and Shaw (1985)
(4) Quartzofeldspathic gneiss, Thackaringa Group, Broken Hill Block, James et al., (1987)
(5) Monzogranite, Kalkadoon Granodiorite, Mt. Isa Block, Wyborn and Page (1983)

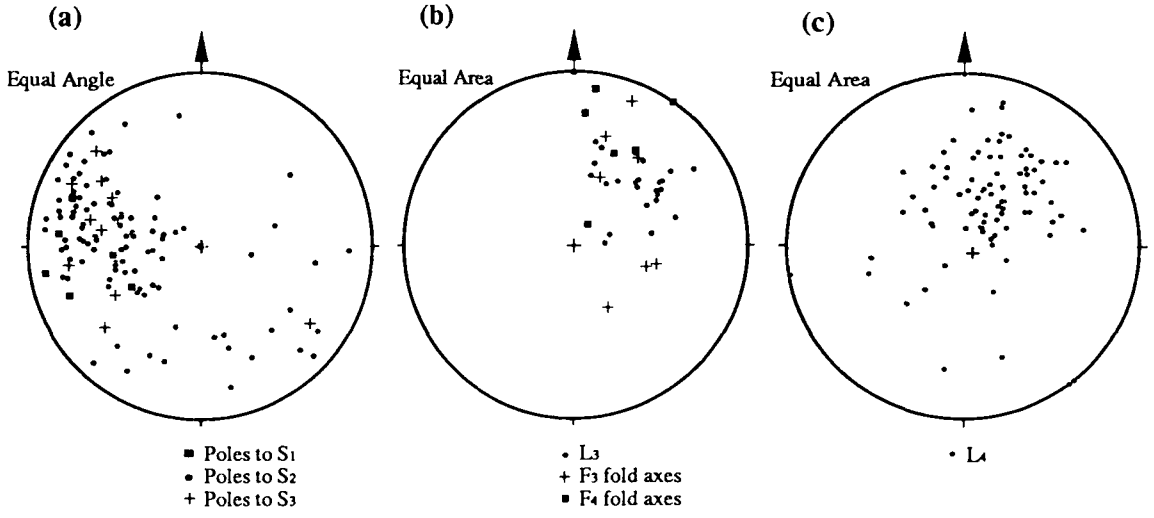


**Fig. 1.6** Structural elements of the Mount Schaber area.
**1.6 (a)** Lower hemisphere, equal angle polar plot of $S_1$, $S_2$ and $S_3$.
**1.6 (b)** Lower hemisphere, equal area stereographic projections of $L_3$ on $S_2$ and $S_1$, and $F_3$ and $F_4$ fold axes.
**1.6 (c)** Lower hemisphere, equal area stereographic projections of mylonitic stretching lineations ($L_4$).

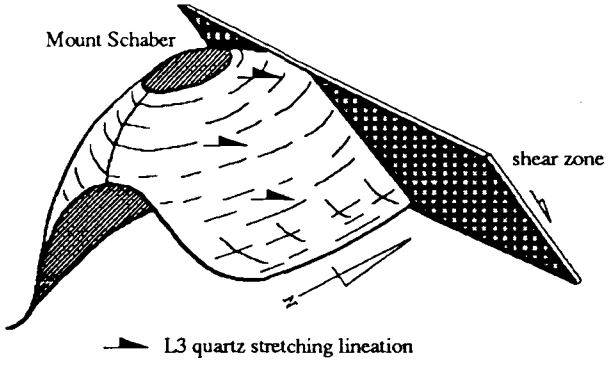


**Fig. 1.7** Sketch of the Mount Schaber antiform.

of coarse-grained quartz-feldspar-biotite leucosome occur in the axial planes of $F_3$ folds (Chapter 2). $F_3$ axial planes dip to the east and southeast and most fold axes plunge up to 50° to the north and northeast. However, some $F_3$ axes also plunge to the southeast (Fig. 1.6b) and there is a broad distribution of $F_3$ axes along a north-south great circle dipping 70° to the east. A well developed quartz stretching lineation ($L_3$), measured on $S_2$, is found throughout the Mount Schaber area and plunges consistently to the northeast, parallel to most $F_3$ axes (Fig. 1.6b). $F_3$ folds are refolded by open, northeast-plunging, inclined, $F_4$ folds. Fine-grained biotite is aligned in the axial plane of some $F_4$ folds and a weak quartz elongation may also define an axial planar fabric. Most $F_3$ and $F_4$ axes are colinear with a mean plunge of 48° to 041. Quartz-feldspar-biotite pegmatite dykes cut both $F_3$ and $F_4$ folds and are displaced by north-dipping $D_4$ ultramylonite zones. Most $D_4$ ultramylonite zones preserve a north-side down sense of shear and well developed stretching lineation ($L_4$) plunging to the northeast.

North of Mount Schaber, $D_4$ ultramylonite zones and $S_2$ gneissosity are cut by a close-spaced, north-dipping, coarse-grained biotite foliation. This foliation forms the pervasive foliation in the Gough Dam Schist Zone (Fig. 1.2). The Gough Dam Schist Zone contains a quartz rodding and a biotite±sillimanite elongation lineation that plunges to the northnortheast. Deformation in the Gough Dam Schist Zone ($D_5$) postdates $D_4$ ultramylonitization and preserves some evidence for south-directed thrusting. Chlorite and muscovite-epidote foliations cut the biotite foliation and commonly have a very oblique to subhorizontal mineral elongation.

### 1.31 The Mount Schaber Antiform (sheath fold)

Mount Schaber consists of a weakly foliated, hypersthene-bearing, quartzofeldspathic granofels that has been macroscopically folded into a doubly plunging, northwest-verging, tight antiform with a curved axial trace (Fig. 1.2). The doubly plunging Mount Schaber antiform is similar to $F_3$ folds in the Ongeva granulites, which contain a well developed, consistent, northeast-plunging, stretching lineation parallel to the fold axes. The axis of the Mount Schaber antiform is curved within the axial plane,

which bends into ultramylonite zones. The axial plane dips about 65° to the southeast and the interlimb angle is 50°. The variation in inclination of the fold axes (*w*) is about 95°. The Mount Schaber antiform folds the $S_1$ compositional layering, $S_2$ leucocratic layering and $S_{2b}$ sillimanite-biotite foliation in the adjacent gneisses. Fig. 1.6a shows the non-cylindrical nature of the Mount Schaber antiform. $S_1$, $S_2$ and $S_3$ in the surrounding gneisses are distributed about a small circle with an axis plunging 60° to 045 and a radius of 75°. $L_3$ plunges everywhere to the northeast (50° to 045) and is colinear with most $F_3$ and $F_4$ folds. $L_3$ has a similar trend to the small circle axis about which $S_1$, $S_2$ and $S_3$ are folded. Minor mafic dykes containing granulite facies assemblages cut the Mount Schaber antiform, suggesting that granulite facies conditions existed during and after folding.

In gneisses adjacent to the Mount Schaber granofels $F_4$ folds are only minor and do not appear to have significantly affected the macroscopic fold pattern. Towards the centre of the folded outcrop of Mount Schaber granofels, no mesoscopic fold interference patterns occur that would suggest interference between a northeast-plunging $F_3$ fold and a northwest-southeast-trending fold. Everywhere in the mount Schaber granofels, an $L_3$ quartz, stretching lineation plunges to the northeast and is not folded. To the south of Mount Schaber, the antiform is discontinuous and the folded $S_2$ foliation becomes parallel with a southeast-trending $D_4$ ultramylonite zone.

Narrow, southeast-trending, discontinuous $D_4$ ultramylonite zones cut the Mount Schaber antiform and are discontinuous with the $S_1$ and $S_2$ in the surrounding gneisses. To the north, the Mount Schaber antiform is dextrally displaced across an ultramylonite zone and the antiform axis and axial plane are bent in a clockwise direction towards the ultramylonitic stretching lineation (Fig. 1.2). The ultramylonite zones dip steeply to the north and contain a fine-grained, northeast-plunging stretching similar to $L_3$ in the Mount Schaber granofels (Fig. 1.6c). Continuous high-strain zones containing a well-developed, southeast-trending foliation ($S_4$) and northeast-plunging, quartz stretching

lineation also cut the Mount Schaber granofels, although little, if any, displacement appears to have occurred across these zones.

The doubly plunging Mount Schaber antiform appears as a curved, oblate '*eye*' structure or tongue (Fig. 1.7) similar to sheath folds that have been described in shear zones and at the base of nappes (Carreras et al., 1977; Cobbold and Quinquis, 1980; Bell and Hammond, 1984; Skjernaa, 1989) as a result of simple shear deformation. The curvature of the Mount Schaber fold axis in the axial plane, the colinearity of stretching lineations and $F_3/F_4$ folds, and the conical distribution of $S_2$ about an axis parallel to the stretching lineation are all features characteristic of mylonitic sheath folds.

## 1.4 The structural and metamorphic history of the Mount Schaber granofels

Mafic granofelses containing two-pyroxene $M_1$ mineral assemblages indicate that metamorphic conditions reached granulite facies during the early part of the tectonic history. Ternary feldspar thermometry (Fuhrman and Lindsley, 1988) indicates peak conditions of at least 825°C at 5 kbar, using an antiperthite bulk composition from the Mount Schaber granofels (Table 1.1). Minerals forming $S_1$, $S_2$, and $S_{2b}$ in gneisses adjacent to Mount Schaber are colinearly folded by tight to isoclinal $F_3$ folds and open $F_4$ folds. These folds probably formed during a continuous, folding episode ($D_3$), which produced the macroscopic fold pattern at Mount Schaber. A northeast plunging $L_3$ quartz stretching lineation is parallel to most $D_3$ fold axes and parallel to the small circle axis about which $S_2$ is folded. The colinearity of $L_3$ and most fold axes indicates a northeast-southwest tectonic transport axis (Shackleton and Ries, 1984) during $D_3$ and implies regional non-coaxial deformation. The doubly plunging Mount Schaber antiform is a macroscopic $F_3$ fold that forms a tight, eye-structure similar to sheath folds in mylonites. $D_3$ is also associated with the intrusion of minor mafic dykes, which probably reflects the thermally perturbed conditions during $D_3$ and suggests that mantle processes may have been involved.

K-poor felsic gneisses and doubly plunging $D_3$ fold closures are not common elsewhere in the Ongeva granulites. This may imply that the unusual composition of the massive Mount Schaber granofels and a rheological contrast with the surrounding interlayered gneisses could have influenced the deformation style that produced the sheath-like $F_3$ antiform. Alternatively, the Mount Schaber antiform may have formed during progressive refolding of an early $D_3$ isoclinal fold, the axis of which was oriented at an oblique angle to the movement direction. Progressive non-coaxial deformation during $D_3$ could have passively rotated the fold axis towards the extension direction (parallel to the stretching lineation) and continual recrystallization would have obliterated any earlier lineations. The tightness of the Mount Schaber antiform would not preclude a rotated origin. To the north of Mount Schaber, the antiform axis and axial plane are bent in a clockwise direction towards a eastnortheast-plunging, stretching lineation in an ultramylonite zone. If a clockwise rotation of an early $D_3$ isoclinal fold occurred, then the preserved northwest antiform fold vergence may indicate that the early deformation involved a southwest-directed tectonic transport.

Felsic, mafic and metapelitic gneisses in the Mount Schaber region preserve $M_2$ microstructures and assemblages that postdate and are texturally distinct from the $M_1$ assemblages and the $S_2$ foliation. In the Mount Schaber granofels, magnesio-hastingsite that rims orthopyroxene, minor biotite clots around titanomagnetite, and scapolite that occurs with myrmekite at recrystallized plagioclase grain boundaries represent the effects of hydration and deformation after $M_1$. Recrystallization, grainsize reduction and symplectites that are attributed to the effects of $M_2$ in mafic granofelses, also occur in mafic micro-enclaves within the Mount Schaber granofels. Therefore, the recrystallized microstructures, grainsize reduction and Cl-rich, hydrous minerals in the Mount Schaber granofels also probably represent the effects of $M_2$. Recrystallized plagioclase (Table 1.1) has a similar composition to $M_1$ antiperthitic plagioclase ($X_{An}$ = 0.33) and two-feldspar thermometry (Stormer, 1975; Brown and Parsons, 1981; Haselton et al., 1983) indicates temperatures of 590±40°C. This probably reflects a blocking temperature to diffusion rather than temperatures during $M_2$ (Chapter 4).

Magnesio-hastingsite, biotite and scapolite are rich in chlorine, suggesting that $M_2$ was accompanied by significant movement of Cl-bearing fluids of unknown origin. An influx of hydrous Cl-bearing fluids through advection during $M_2$ could cause strain softening. This may have contributed to heterogeneous deformation of the Ongeva granulites and development of sheath-like folds, if $D_3$ was concomitant with $M_2$. The tectonic setting of $M_2$ cannot be determined from the petrology of the Mount Schaber granofels, but an influx of Cl-bearing fluids during folding could imply dewatering from a subducted slab. The structure and petrology of the Mount Schaber granofels suggests that $D_3/M_2$ represents a significant, regional, non-coaxial event sometime after cooling from the metamorphic peak, which was unrelated to event(s) that were responsible for $M_1$.

$D_4$ ultramylonitization post-dated folding of the Mount Schaber granofels, but the similar trend of $L_3$ and stretching lineations in the shear zones suggests that ultramylonitization may have been associated with $D_3$ folding. The shear zones preserve a north-side down sense of shear and may represent syn- and post-$D_3$ compressional extension (Chapter 5).

## 1.5 Nature of the protolith and the effects of fluid

The problems of recognizing precursors, particularly for felsic gneisses in high-grade metamorphic terrains, and of discriminating tectonic settings are difficult because of migmatization and recrystallization during metamorphism (Vernon and Williams, 1988). Any field evidence for a volcanic or sedimentary origin for the rocks at Mount Schaber has been obliterated by deformation and recrystallization. However, the tectonic setting for precursor rocks in the Ongeva granulites may be interpreted using the geochemistry of interlayered mafic and metapelitic gneisses.

The geochemistry of mafic and metapelitic gneisses, and the lack of rocks of intermediate composition in the Ongeva granulites suggest that these gneisses were derived from a rifted continental margin or in intra-continental rift tectonic setting. Mafic

granofelses and gneisses, which are interlayered with felsic gneisses in the Ongeva granulites, are subalkaline-basalts to basaltic-andesites in composition (Fig. 1.5c), olivine-normative and tholeiitic, with a moderate $TiO_2$ content (1.30%, Table 1.3; average analysis). They have a normative mineralogy (Fig. 1.8a) and Y-Cr content (Fig. 1.8b) that are similar to those of MOR basalts (Pearce et al., 1984). The moderate $TiO_2$ content may also discriminate them from low-Ti island arc basaltic andesites (Ewart et al., 1973). The mafic rocks in the Ongeva granulites are similar to other LREE-depleted metatholeiites, east of the study area, which resemble MOR basalts and some continental tholeiites (Sivell, 1988). Metapelites interlayered with mafic and felsic gneisses have high averaged abundances of La (57 ppm), Th (26 ppm), and U (1.2 ppm, Table 1.3), reflecting a probable continental erosional source rather than an arc-derived source (Bhatia and Taylor, 1981). They have a low La/Th ratio (> 2.0, Fig. 1.8c), which is similar to clastic sedimentary rocks found at rifted continental margins and in marginal basins (Bhatia and Taylor, 1981), and unlike rocks with an andesitic source. Metapelites are also $SiO_2$-poor, which probably reflects a low abundance of quartz detritus, and contain a significant content of elements that occur in plagioclase (i.e. Ca, Na and Sr) and not in clay minerals (Wyborn and Chappell, 1983), which reflects an immature erosional source.

The composition of most felsic gneisses from the Ongeva granulites is typical of many Australian Proterozoic igneous rocks of similar-age, which are high in $K_2O$ and REE, relative to modern igneous rocks (Wyborn et al., 1987). Warren and Shaw (1985) interpreted the well-layered felsic gneisses of the Strangways Metamorphic Complex to be distal (flank and apron) volcanogenic deposits and the more massive granofelses to be minor proximal units. K-poor, REE depleted felsic gneisses appear to be anomalous in the Ongeva granulites and are unlike the composition of other Australian Proterozoic igneous rocks and most unaltered Phanerozoic igneous rocks. Therefore, the geochemistry of these anomalous rocks may reflect processes other than inheritance of a source rock composition.

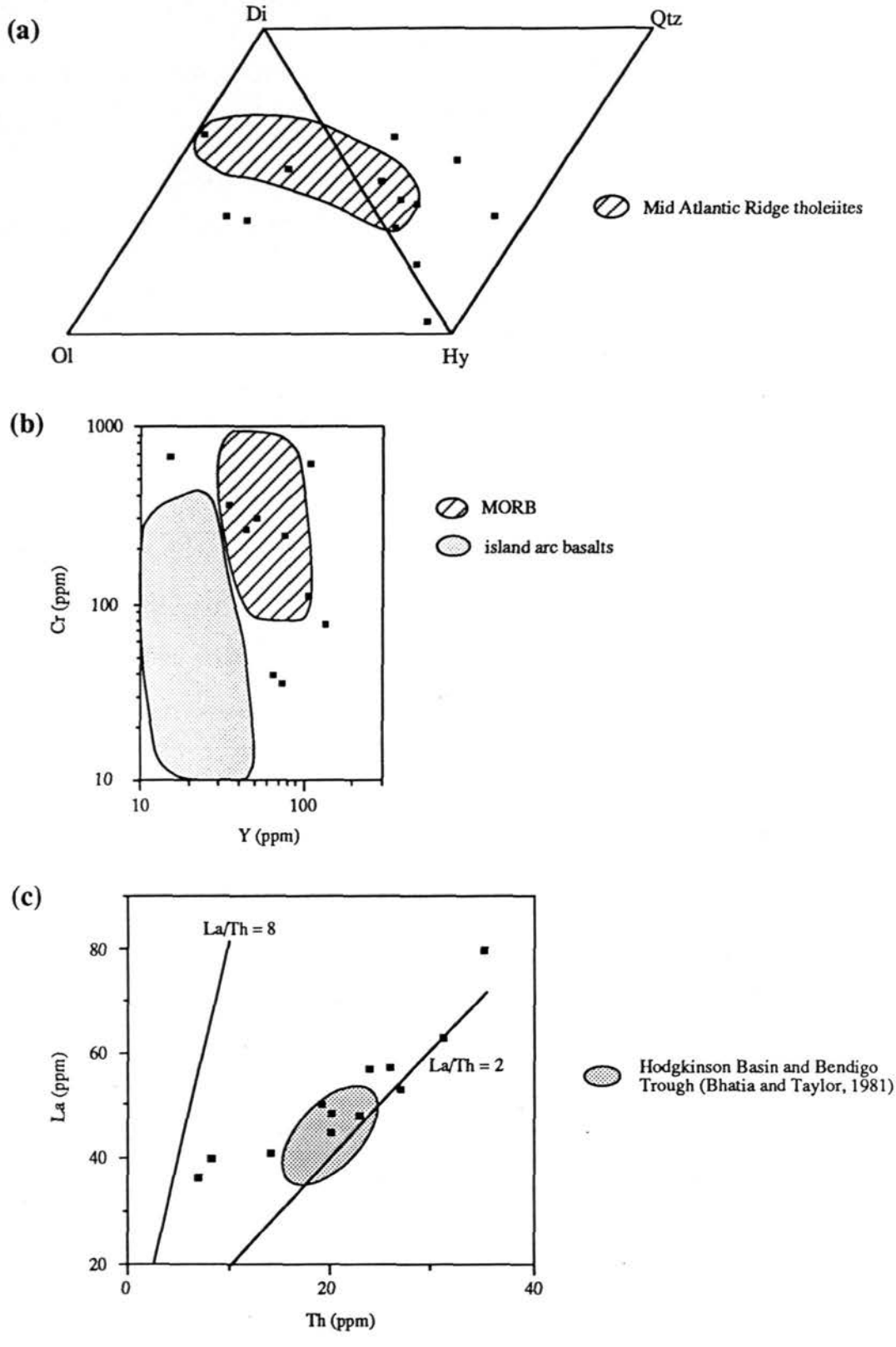


**Fig. 1.8 (a)** Normative mineralogy of mafic gneisses and granofelses from the Ongeva ganulites, showing field of Mid-Atlantic Ridge tholeiites (Schilling, 1975).

**1.8 (b)** Plot of Y versus Cr for mafic gneisses and granofelses from the Ongeva ganulites, showing field of MOR basalts and island arc basalts (Pearce et al., 1984).

**1.8 (c)** Plot of Th versus La for metapelites from the Ongeva granulites, showing the field of Hohgkinson Basin and Bendigo Trough sedimentary rocks (Bhatia and Taylor, 1981).

Ti, Zr, Y, and Nb are elements with a high field strength, which are not readily transported in aqueous fluids. They may be helpful in determining the source from which granitic rocks were derived and discriminating between different tectonic settings in which they intruded (Pearce and Norry, 1979, Pearce et al, 1984). In the Mount Schaber granofels and adjacent felsic gneisses, Ti, Zr, and Nb decrease with increasing $SiO_2$ content, possibly reflecting fractional differentiation from a common source. However, Y content appears to be unrelated to $SiO_2$, $TiO_2$ and Zr (Fig. 1.5d) content. The variation of Y may reflect some degree of chemical mobility. Transportation of Y in fluids over short distances could occur when the fluid contains high activities of agents such as Cl or F ( Pearce and Norry, 1979). The high Cl content in amphibole, scapolite and biotite in the Mount Schaber felsic granofels suggests that the activity of Cl was probably high during $M_2$ hydration. The least microscopically recrystallized samples at Mount Schaber contain few of the Cl-rich retrograde minerals and appear to be less Y-depleted. This implies that Y may have been preferentially removed from the more deformed rocks during fluid movement and that Cl was scavenged from the fluid by minerals that formed during retrogression. Alternatively, the Mount Schaber granofels and adjacent felsic gneisses could have been deposited as tephras with a variable clastic component containing Y. In these circumstances, variable depletion in other REE may be expected.

Page et al. (1984) noted a contemporaneity of igneous activity and crustal deformation throughout the Proterozoic of Australia. Wyborn et al. (1987) divided the Proterozoic igneous activity of Australia into 6 major igneous periods, two of which were associated with deformational events (1870-1840 Ma and ~1600 Ma), the others being associated with the formation of major sedimentary basins. The oldest metamorphic event recorded in the Strangways Metamorphic Complex occurred around 1800 Ma ago (Iyer et al., 1976; Black et al., 1983; Windrim and McCulloch, 1986), the crustal formation model age being estimated at about 2000 Ma (Windrim and McCulloch, 1986). Felsic rocks with ages in the 2000-1870 Ma and 1870-1840 Ma periods are characterized by high $K_2O$, Rb, La, Ce, Th, U and low MgO, CaO, Ni and Cr, compared to modern

analogues (Wyborn et al., 1987; Wyborn, 1989). Most of the Mount Schaber samples differ from other typical Australian Proterozoic felsic rocks (Table 1.5) in being depleted in $K_2O$, Rb and Ba and slightly enriched in $SiO_2$. However, the composition of other felsic gneisses from the Ongeva granulites and Strangways Metamorphic Complex (Tables 1.4 and 1.5) is more typical of Australian Proterozoic felsic rocks (Table 1.5, Wyborn et al., 1987; James et al., 1987; Wyborn and Page, 1983), and have higher $K_2O$ and Rb content than the Mount Schaber samples. Although the Mount Schaber granofels and felsic gneisses have an "I-type" chemical composition (Chappell and White, 1974), which suggests they formed from an igneous protolith, they are also compositionally unlike many unaltered Phanerozoic felsic igneous rocks (White and Chappell, 1983). The paucity of analogies with Proterozoic felsic gneisses and unaltered Phanerozoic granites and rhyolites suggests that the unusual composition on the Mount Schaber granofels and felsic gneisses could be explained by alteration processes.

K-poor felsic granofelses similar to those at Mount Schaber have been also described from the Utnalanama Block (Allen, 1979), south of the Strangways Metamorphic Complex. Allen (1979) suggested that their chemistry was indicative of $K_2O$ depletion during granulite facies metamorphism. The felsic granofelses at Mount Schaber differ from the Utnalanama Block felsic gneisses in being considerably lower in Ba and lower in MgO. In contrast to the observations of Allen (1979), an unsystematic compositional variation, even within a single stratigraphic unit, has been observed in felsic gneisses from the Ongeva granulites, rather than a widespread $K_2O$ depletion. Similar compositional variations occur in quartzofeldspathic rocks from Broken Hill (Brown et al., 1983). K-poor, Na-rich, cm-thick layers in these rocks have been interpreted as keratophyric tuffs or metamorphosed analcimized airfall tuff (Brown et al., 1983). Analcime rocks with a similar K-poor composition but higher $Na_2O$ composition to the Mount Schaber granofels have been described from the Green River Formation, U. S. A (Coombs, 1965). Bradley (1929) interpreted the analcime in the Green River Formation, as an alteration of ash in saline lake water. The local mobility of alkalies is also common in hydrothermally altered siliceous and mafic volcanic rocks

(Vallance, 1967). Seawater, saline lake water or hydrothermal alteration may be expected in a continental rift setting. If the more massive, felsic granofelses in the Ongeva granulites, such as the Mount Schaber granofels represent more proximal deposits in a rift setting, hydrothermal alteration would be common. However, the K-poor composition of felsic rocks at Mount Schaber does not necessarily imply an anorogenic style of magmatism and alteration, because low-K dacites and rhyolites have also been recorded from active island arc settings (e.g. Metis Shoal, Tonga, Ewart et al 1973; South Sandwich Islands, Gass et al., 1963).

Although the geochemistry of Phanerozoic granitic rocks may discriminate between different tectonic settings (Pearce et al., 1984; Harris et al., 1986), the interpretation of a tectonic setting for the Mount Schaber samples cannot be well constrained. The felsic rocks at Mount Schaber plot in both the volcanic arc and within-plate granite fields (Pearce et al., 1984) on Nb-Y and Rb-(Y+Nb) diagrams (Fig. 1.9). The samples that plot within the volcanic arc field probably reflect partial depletion of Y and Rb. The rocks, which are least depleted in Y and least deformed plot in the within-plate granite field and are more likely to indicate the tectonic setting in which the Ongeva granulites formed. However, other felsic gneisses from the Ongeva granulites also have compositions that plot between the volcanic arc and within-plate granite fields (Fig. 1.9) of Pearce et al. (1984). The geochemistry of mafic rocks and metapelites suggests that a continental rift setting is more likely that a volcanic arc tectonic setting, and the compositional extension of felsic rocks to mafic compositions (Fig. 1.5c) suggests that the Ongeva granulites were partly mantle derived and did not have an evolved continental crustal source. The plot of Nb-Y and Rb-(Y+Nb) for felsic rocks in the Ongeva granulites and an interpreted continental rift setting may imply that the discrimination fields for Proterozoic granitic rocks is different to that for Phanerozoic rocks. It has been suggested that an expansion of the volcanic arc field through time could reflect a crustal enrichment in Nb and Y during evolution of the crust (Foden et al., 1988). A within plate field that included felsic gneiss compositions from the Ongeva

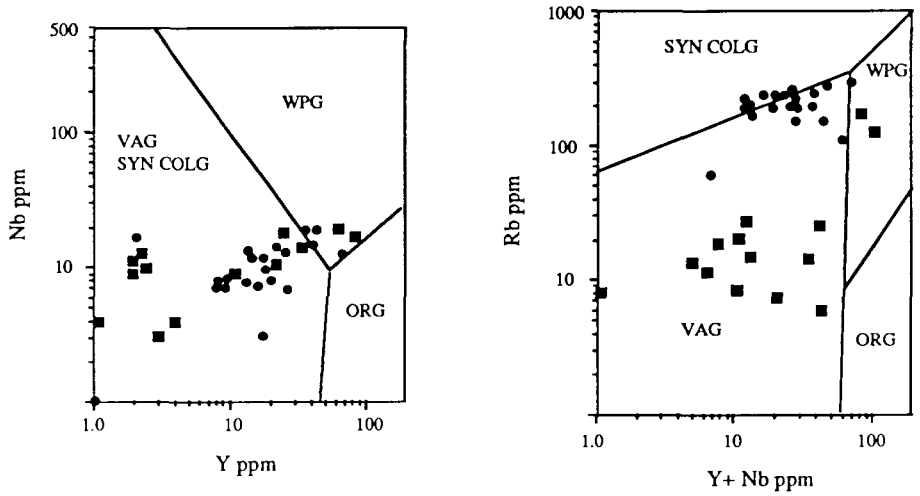


• Felsic gneisses from the Ongeva granulites

▪ Mount Schaber granofels and adjacent felsic gneisses

**Fig. 1.9** Nb-Y and Rb-(Nb + Y) discriminant diagrams (Pearce et al., 1984) for felsic rocks at Mount Schaber and felsic gneisses from the Ongeva granulites.
VAG - volcanic arc granites, SYN COLG - syncollisional granites, WPG - within plate granites, ORG - ocean ridge granites

granulites would imply a contracted volcanic arc field in the Proterozoic and suggests that the Proterozoic crust was depleted in Nb and Y compared with the Phanerozoic crust.

Low-K, REE-depleted granites and gneisses are common in Archean terrains (Martin et al., 1983) but these rocks generally have a higher $Al_2O_3$ content compared with the Mount Schaber felsic rocks. The composition of low-K felsic Archean rocks has been attributed to partial melting of a mantle-crustal source with a garnet residual at pressures of > 12 kbar (Rapp et al., 1991). However, the effects of alteration on Archean felsic rocks also appears to be poorly understood. Supracrustal rocks interlayered with the Mount Schaber granofels and the characteristic bimodal composition of the Strangways Metamorphic Complex suggest that they formed a conformable sequence in a volcanic pile. Moreover, there is no evidence for an early high-pressure, high-temperature metamorphism (Warren and Stewart, 1988; Clarke and Powell, 1991; Norman and Clarke, 1990) in the Arunta Block to suggest that the low-K composition of the Mount Schaber granofels could be explained by high-pressure crustal melting.

High-grade metamorphism ($M_1$ and $M_2$) of the Mount Schaber granofels and adjacent felsic gneisses was accompanied by the formation of migmatites and modification of the bulk rock chemical composition. The development of myrmekite in $M_2$ microstructures indicates some mobility of K over at least short distances and the presence of chlorine-bearing, hydrous retrograde minerals indicates that recrystallization and retrogression after the metamorphic peak involved a Cl-bearing fluid phase. Although these features make it difficult to recognize the precursors of the Mount Schaber granofels and adjacent felsic gneisses, the samples have chemical analogies with altered tephras from the Newcastle Coal Measures and analcime rocks from Green River Formation. The rocks also show significant differences from other typical Proterozoic felsic gneisses and Phanerozoic felsic igneous rocks, which suggest that the unusual chemical composition of the Mount Schaber felsic rocks may be explained by diagenetic alteration of a glassy rhyolitic precursor. Compositional variations within the Mount Schaber granofels may be due to heterogeneous alteration of a volcanic unit and

differences in the mineral composition of a diagenetically altered precursor (e.g. analcime-quartz±calcite or quartz-adularia?). The unsystematic variation of Y with rock composition may reflect a high activity of Cl in a fluid phase during a major, tectonometamorphic event that produced the sheath-like fold pattern. Fluid movement during deformation would assist in strain softening and the development of a regional non-coaxial deformation.

**Appendix 1-A** Whole-rock analyses from felsic gneisses in the Ongeva granulites.

| wt% | 12 C | 14B | 15 | 16 | 17 | 18A | 18B | 19 | 25 | 31 | 30 | 36 | 37 | 38 | 39 B | 45 | 48A | 49A | 50 | 54 | average |
|---|---|---|---|---|---|---|---|---|---|---|---|---|---|---|---|---|---|---|---|---|---|
| $SiO_2$ | 73.38 | 75.82 | 72.82 | 73.43 | 73.15 | 71.38 | 75.16 | 72.85 | 73.01 | 73.89 | 73.54 | 73.09 | 73 | 72.02 | 73.93 | 75.38 | 70.73 | 70.54 | 74.73 | 72.05 | 73.20 |
| $TiO_2$ | 0.42 | 0.41 | 0.48 | 0.4 | 0.42 | 0.6 | 0.6 | 0.46 | 0.04 | 0.03 | 0.5 | 0.3 | 0.51 | 0.44 | 0.44 | 0.14 | 0.65 | 0.66 | 0.28 | 0.42 | 0.41 |
| $Al_2O_3$ | 12.63 | 12.33 | 12.56 | 13.02 | 12.75 | 12.07 | 13.53 | 12.58 | 14.38 | 14.33 | 12.24 | 12.47 | 12.5 | 12.73 | 12.9 | 13.13 | 13.87 | 12.6 | 11.71 | 12.5 | 12.84 |
| $Fe_2O_3$ | 1.8 | 0.57 | 1.44 | 0.74 | 1.79 | 2.16 | 0.29 | 1.59 | 0.2 | 0.06 | 1.5 | 1.87 | 1.35 | 1.92 | 0.97 | 0.51 | 1.33 | 3.22 | 0.65 | 2.74 | 1.33 |
| FeO | 1.24 | 0.58 | 1.83 | 1.31 | 1.48 | 2.72 | 0.56 | 1.49 | 0.1 | 0.13 | 1.65 | 0.93 | 1.68 | 1.79 | 1.38 | 0.74 | 1.9 | 2.55 | 1.46 | 2.22 | 1.39 |
| MnO | 0.02 | 0.02 | 0.02 | 0.03 | 0.03 | 0.02 | 0.02 | 0.01 | 0.01 | 0.01 | 0.01 | 0.01 | 0.01 | 0.02 | 0.02 | 0.03 | 0.04 | 0.04 | 0.02 | 0.03 | 0.02 |
| MgO | 0.44 | 0.26 | 0.69 | 0.66 | 0.56 | 1.04 | 0.13 | 0.67 | 0.08 | 0.03 | 0.36 | 0.34 | 0.73 | 0.62 | 0.66 | 0.26 | 0.7 | 0.81 | 1.1 | 0.22 | 0.52 |
| CaO | 1.37 | 1.85 | 1.56 | 1.61 | 1.45 | 0.71 | 3.07 | 1.65 | 0.59 | 0.51 | 1.19 | 0.14 | 1.64 | 1.37 | 1.36 | 1.3 | 1.78 | 2.07 | 0.71 | 0.29 | 1.31 |
| $Na_2O$ | 2.64 | 3.28 | 2.22 | 2.22 | 2.4 | 1.9 | 3.4 | 2.05 | 1.76 | 1.43 | 1.71 | 1.37 | 2.34 | 2.33 | 3.08 | 2.76 | 2.08 | 2.37 | 1.6 | 1.22 | 2.21 |
| $K_2O$ | 5.12 | 4.12 | 5.53 | 5.82 | 5.27 | 6.3 | 2.24 | 5.46 | 9.05 | 9.34 | 6.31 | 8.76 | 5.32 | 5.83 | 4.37 | 5.4 | 6.43 | 4.24 | 6.74 | 8.01 | 5.98 |
| $P_2O_4$ | 0.07 | 0.02 | 0.08 | 0.11 | 0.08 | 0.1 | 0.01 | 0.06 | 0.04 | 0.02 | 0.07 | 0.04 | 0.09 | 0.08 | 0.07 | 0.04 | 0.14 | 0.13 | 0.02 | 0.06 | 0.07 |
| $H_2O+$ | 0.29 | 0.21 | 0.31 | 0.29 | 0.31 | 0.44 | 0.27 | 0.27 | 0.26 | 0.28 | 0.43 | 0.32 | 0.31 | 0.28 | 0.46 | 0.32 | 0.44 | 0.38 | 0.44 | 0.17 | 0.32 |
| $H_2O-$ | 0.01 | 0.04 | 0.08 | 0.04 | 0.03 | 0.02 | 0.13 | 0.08 | 0.14 | 0.03 | 0.1 | 0.08 | 0.06 | 0.09 | 0.1 | 0.04 | 0.11 | 0.02 | 0.1 | 0.05 | 0.07 |
| $CO_2$ | 0.01 | 0.06 | 0.15 | 0.16 | 0.03 | 0.04 | 0.18 | 0.02 | 0.06 | 0.05 | 0.07 | 0.01 | 0.11 | 0.06 | 0.04 | 0.03 | 0.05 | 0.03 | 0.09 | 0.03 | 0.06 |
| TOTAL | 99.44 | 99.57 | 99.77 | 99.84 | 99.77 | 99.49 | 99.59 | 99.24 | 99.72 | 100.15 | 99.68 | 99.73 | 99.65 | 99.59 | 99.77 | 100.08 | 100.25 | 99.67 | 99.65 | 100.02 | 99.73 |
| S.I. index* | 1.02 | 0.93 | 1.01 | 1.01 | 1.04 | 1.07 | 1.00 | 1.02 | 1.05 | 1.07 | 1.04 | 1.04 | 0.99 | 1.01 | 1.05 | 1.03 | 1.02 | 1.03 | 1.04 | 1.12 | 1.03 |
| trace elements (ppm) | | | | | | | | | | | | | | | | | | | | | |
| Ba | 714 | 942 | 770 | 893 | 719 | 1195 | 109 | 858 | 2090 | 1607 | 1561 | 1230 | 837 | 815 | 725 | 464 | 1510 | 862 | 1110 | 1150 | 1008 |
| Ce | 102 | 58 | 59 | 32 | 83 | 99 | 25 | 121 | 24 | 29 | 87 | 52 | 42 | 76 | 29 | 90 | 39 | 94 | 92 | 85 | 66 |
| Cr | 8 | 4 | 9 | 9 | 10 | 10 | 8 | 10 | 6 | 3 | 3 | 6 | 12 | 11 | 7 | 4 | 4 | 7 | 2 | 11 | 7 |
| Cu | 19 | 11 | 27 | 21 | 18 | 30 | 12 | 16 | 16 | 19 | 32 | 20 | 21 | 24 | 21 | 13 | 22 | 26 | 16 | 25 | 20 |
| Ga | 15 | 16 | 16 | 14 | 16 | 15 | 18 | 15 | 11 | 11 | 15 | 11 | 15 | 17 | 17 | 14 | 14 | 18 | 12 | 14 | 15 |
| La | 45 | 19 | 30 | 18 | 46 | 54 | 5 | 66 | 16 | 11 | 45 | 26 | 18 | 36 | 10 | 66 | 15 | 50 | 46 | 41 | 33 |
| Nb | 13 | 17 | 7 | 7 | 13 | 7 | 18 | 7 | 1 | 1 | 12 | 8 | 12 | 8 | 12 | 3 | 8 | 12 | 14 | 10 | 10 |
| Nd | 40 | 34 | 27 | 19 | 39 | 36 | 11 | 50 | 12 | 15 | 34 | 28 | 17 | 34 | 17 | 40 | 26 | 41 | 43 | 36 | 30 |
| Ni | 8 | 1 | 8 | 10 | 10 | 14 | 3 | 9 | 10 | 10 | 13 | 13 | 11 | 12 | 9 | 5 | 18 | 8 | 3 | 14 | 9 |
| Pb | 11 | 8 | 14 | 6 | 12 | 11 | 5 | 13 | 29 | 14 | 8 | 13 | 6 | 10 | 5 | 36 | 12 | 7 | 9 | 8 | 12 |
| Pr | 14 | 0 | 6 | 0 | 11 | 11 | 0 | 18 | 0 | 0 | 10 | 0 | 0 | 11 | 0 | 17 | 0 | 14 | 16 | 9 | 7 |
| Rb | 240 | 107 | 213 | 236 | 260 | 237 | 53 | 216 | 269 | 312 | 199 | 265 | 215 | 235 | 159 | 256 | 190 | 162 | 272 | 291 | 219 |
| Sr | 66 | 114 | 71 | 92 | 62 | 107 | 128 | 80 | 106 | 135 | 84 | 57 | 89 | 77 | 105 | 54 | 130 | 99 | 82 | 41 | 89 |
| Th | 22 | 26 | 12 | 2 | 28 | 31 | 23 | 38 | 3 | 4 | 28 | 39 | 3 | 29 | 17 | 31 | 3 | 17 | 36 | 34 | 21 |
| U | 2 | 1 | 3 | 2 | 2 | 3 | 3 | 3 | 2 | 2 | 3 | 2 | 2 | 3 | 1 | 4 | 2 | 1 | 3 | 4 | 2 |
| V | 16 | 10 | 23 | 18 | 17 | 17 | 11 | 24 | 7 | 4 | 19 | 13 | 36 | 22 | 14 | 11 | 52 | 16 | 7 | 20 | 18 |
| Y | 23 | 49 | 9 | 8 | 33 | 17 | 2 | 8 | 0 | 0 | 26 | 12 | 13 | 20 | 15 | 18 | 8 | 32 | 14 | 68 | 19 |
| Zn | 23 | 11 | 19 | 15 | 28 | 19 | 5 | 17 | 8 | 9 | 12 | 7 | 11 | 12 | 11 | 14 | 27 | 41 | 15 | 4 | 15 |
| Zr | 260 | 382 | 288 | 244 | 270 | 401 | 397 | 294 | 21 | 9 | 379 | 174 | 314 | 252 | 289 | 107 | 144 | 422 | 298 | 287 | 262 |
| CIPW norms | | | | | | | | | | | | | | | | | | | | | |
| Qtz | 35.01 | 37.3 | 34.36 | 34.01 | 35.11 | 32.51 | 40.56 | 35.4 | 27.06 | 28.81 | 36.3 | 30.93 | 34.48 | 32.22 | 35.22 | 35.35 | 29.06 | 34.87 | 36.03 | 33.06 | 33.86 |
| Or | 30.26 | 24.33 | 32.68 | 34.4 | 31.14 | 37.23 | 13.24 | 32.26 | 53.46 | 55.19 | 37.29 | 51.76 | 31.42 | 34.45 | 25.82 | 31.88 | 38 | 25.06 | 39.8 | 47.33 | 35.34 |
| Ab | 22.33 | 27.72 | 18.79 | 18.78 | 20.31 | 16.08 | 28.77 | 17.34 | 14.89 | 12.1 | 14.47 | 11.6 | 19.8 | 19.72 | 26.06 | 23.35 | 17.6 | 20.05 | 13.54 | 10.32 | 18.70 |
| An | 6.24 | 6.78 | 6.27 | 6.29 | 6.48 | 2.62 | 14.03 | 7.7 | 2.29 | 2.08 | 5 | 0.36 | 6.86 | 5.89 | 6.04 | 6.02 | 7.6 | 9.23 | 2.81 | 0.86 | 5.66 |
| Crn | 0.46 | 0 | 0.63 | 0.76 | 0.72 | 1.17 | 0.37 | 0.47 | 0.85 | 1.1 | 0.76 | 0.6 | 0.38 | 0.43 | 0.89 | 0.54 | 0.7 | 0.73 | 0.75 | 1.51 | 0.66 |
| Di | 0 | 1.38 | 0 | 0 | 0 | 0 | 0 | 0 | 0 | 0 | 0 | 0 | 0 | 0 | 0 | 0 | 0 | 0 | 0 | 0 | 0 |
| Hy | 1.24 | 0 | 3.13 | 2.82 | 2 | 4.85 | 0.32 | 2.36 | 0.19 | 0.23 | 1.88 | 0.85 | 2.96 | 2.56 | 2.69 | 1.4 | 3.13 | 3.02 | 4.43 | 1.72 | 2.11 |
| Mag | 2.61 | 0.74 | 2.09 | 1.07 | 2.6 | 3.13 | 0.13 | 2.31 | 0.24 | 0.09 | 2.17 | 2.18 | 1.96 | 2.78 | 1.41 | 0.74 | 1.93 | 4.67 | 0.95 | 3.97 | 1.93 |
| Ilm | 0.79 | 0.79 | 0.91 | 0.76 | 0.8 | 1.14 | 1.14 | 0.87 | 0.07 | 0.06 | 0.95 | 0.56 | 0.97 | 0.84 | 0.84 | 0.26 | 1.23 | 1.25 | 0.54 | 0.8 | 0.78 |
| Ap | 0.18 | 0.05 | 0.19 | 0.25 | 0.19 | 0.24 | 0.02 | 0.13 | 0.09 | 0.05 | 0.17 | 0.09 | 0.21 | 0.19 | 0.17 | 0.09 | 0.33 | 0.31 | 0.05 | 0.14 | 0.17 |

* molecular $Al_2O_3/(Na_2O+K_2O+CaO)$

**Appendix 1-B** Whole-rock analyses from mafic gneisses and granofelses in the Ongeva granulites.

| wt% | 10 | 13A | 21 | 40 | 42 | 43 | 44B | 48B | 49C | 51 | ultramafic 955 | average | mafic dyke 912 |
|---|---|---|---|---|---|---|---|---|---|---|---|---|---|
| $SiO_2$ | 47.78 | 50.44 | 51.52 | 47.74 | 54.77 | 49.56 | 50.63 | 54.39 | 47.11 | 50.8 | 49.96 | 50.43 | 48.07 |
| $TiO_2$ | 1.42 | 2.65 | 1.56 | 2.11 | 1.44 | 0.73 | 1.36 | 1.55 | 0.72 | 0.55 | 0.16 | 1.30 | 0.73 |
| $Al_2O_3$ | 15.11 | 15.36 | 15.67 | 14.04 | 14.46 | 20.41 | 14.58 | 14.65 | 14.74 | 15.76 | 7.92 | 14.79 | 14.67 |
| $Fe_2O_3$ | 3.28 | 2.14 | 4.98 | 4 | 2.94 | 1.92 | 4.84 | 4.45 | 3.62 | 1.54 | 1.70 | 3.22 | 4.12 |
| FeO | 10.09 | 6.46 | 9.07 | 10.31 | 7.57 | 4.9 | 9.37 | 8.84 | 11.19 | 9.54 | 2.94 | 8.21 | 9.98 |
| MnO | 0.16 | 0.09 | 0.08 | 0.16 | 0.08 | 0.07 | 0.17 | 0.18 | 0.15 | 0.15 | 0.15 | 0.13 | 0.24 |
| MgO | 7.9 | 7.6 | 6.47 | 6.7 | 5.13 | 5.51 | 5.53 | 3.39 | 8.58 | 9.02 | 13.85 | 7.24 | 7.75 |
| CaO | 10.41 | 9.39 | 8.3 | 9.46 | 9.24 | 12.52 | 8.82 | 7.41 | 8.84 | 9.12 | 22.81 | 10.57 | 9.55 |
| $Na_2O$ | 1.44 | 1.9 | 1.18 | 2.83 | 3.2 | 2.98 | 2.99 | 3.32 | 2.18 | 2.08 | 0.21 | 2.21 | 2.90 |
| $K_2O$ | 0.76 | 2.01 | 0.39 | 0.94 | 0.58 | 0.55 | 0.71 | 0.69 | 1.08 | 0.22 | 0.11 | 0.73 | 0.42 |
| $P_2O_4$ | 0.22 | 0.02 | 0.19 | 0.42 | 0.05 | 0.03 | 0.16 | 0.32 | 0.04 | 0.04 | 0.03 | 0.14 | 0.08 |
| $H_2O+$ | 0.73 | 1.22 | 0.31 | 0.6 | 0.32 | 0.47 | 0.33 | 0.4 | 0.75 | 0.32 | 0.59 | 0.55 | 0.68 |
| $H_2O-$ | 0.07 | 0.06 | 0.03 | 0.04 | 0.03 | 0.04 | 0.04 | 0.03 | 0.06 | 0.05 | 0.13 | 0.05 | 0.15 |
| $CO_2$ | 0.3 | 0.08 | 0.12 | 0.13 | 0.02 | 0.06 | 0.14 | 0.17 | 0.05 | 0.19 | 0.01 | 0.12 | 0.10 |
| TOTAL | 99.66 | 99.43 | 99.86 | 99.48 | 99.84 | 99.75 | 99.69 | 99.79 | 99.12 | 99.38 | 100.55 | 99.69 | 99.44 |
| trace elements (ppm) | | | | | | | | | | | | | |
| Ba | 54 | 243 | 50 | 118 | 52 | 81 | 180 | 194 | 232 | 45 | 21 | 115 | 111 |
| Ce | 24 | 33 | 74 | 61 | 28 | 23 | 66 | 61 | 135 | 0 | | 46 | |
| Cr | 365 | 40 | 242 | 271 | 113 | 306 | 81 | 35 | 635 | 704 | 1 | 254 | 228 |
| Cu | 89 | 32 | 70 | 82 | 34 | 31 | 72 | 68 | 32 | 60 | 3 | 52 | 75 |
| Ga | 18 | 19 | 23 | 20 | 23 | 18 | 24 | 19 | 21 | 16 | 12 | 19 | 20 |
| La | 17 | 8 | 32 | 34 | 8 | 0 | 23 | 26 | 59 | 0 | | 19 | |
| Nb | 4 | 8 | 9 | 8 | 16 | 5 | 19 | 17 | 21 | 2 | 9 | 11 | 2 |
| Nd | 14 | 19 | 46 | 27 | 13 | 12 | 50 | 30 | 70 | 0 | | 26 | |
| Ni | 106 | 53 | 65 | 109 | 45 | 50 | 59 | 32 | 148 | 177 | 13 | 78 | 214 |
| Pb | 10 | 7 | 8 | 7 | 5 | 6 | 7 | 8 | 7 | 5 | 9 | 7 | 7 |
| Pr | 6 | 0 | 12 | 9 | 0 | 0 | 15 | 11 | 26 | 0 | | 7 | |
| Rb | 12 | 179 | 11 | 12 | 3 | 12 | 5 | 6 | 23 | 7 | 4 | 25 | 19 |
| Sr | 100 | 115 | 68 | 117 | 118 | 199 | 120 | 135 | 80 | 92 | 4 | 104 | 103 |
| Th | 2 | 2 | 3 | 3 | 0 | 2 | 0 | 0 | 4 | 1 | 7 | 2 | 2 |
| U | 1 | 2 | 2 | 2 | 1 | 1 | 2 | 2 | 2 | 2 | 2 | 2 | 0 |
| V | 294 | 624 | 348 | 247 | 167 | 175 | 271 | 170 | 199 | 169 | 19 | 244 | 237 |
| Y | 34 | 65 | 75 | 43 | 106 | 50 | 133 | 72 | 108 | 15 | 106 | 73 | 24 |
| Zn | 59 | 43 | 41 | 64 | 19 | 23 | 90 | 121 | 71 | 70 | 313 | 83 | 94 |
| Zr | 65 | 39 | 87 | 101 | 153 | 60 | 135 | 212 | 49 | 29 | 155 | 99 | 39 |
| CIPW norms | | | | | | | | | | | | | |
| Qtz | 1 | 4.57 | 12.63 | 0 | 7.24 | 0 | 2.88 | 10.46 | 0 | 0.75 | 0.00 | 2.53 | 0.00 |
| Or | 4.49 | 4.49 | 2.31 | 5.56 | 3.46 | 3.24 | 4.18 | 4.1 | 6.41 | 1.29 | 0.00 | 4.31 | 2.48 |
| Ab | 12.21 | 12.18 | 9.96 | 23.95 | 27.07 | 25.23 | 25.32 | 28.08 | 18.46 | 17.58 | 0.00 | 18.70 | 24.54 |
| An | 32.49 | 32.52 | 36.3 | 22.8 | 23.35 | 40.67 | 24.25 | 23.02 | 27.23 | 33.02 | 20.34 | 28.28 | 25.77 |
| Crn | 0 | 0 | 0 | 0 | 0 | 0 | 0 | 0 | 0 | 0 | 0.00 | 0.00 | 0.00 |
| Di | 12.92 | 12.85 | 2.35 | 16.81 | 18.02 | 16.83 | 14.43 | 8.82 | 13.15 | 8.78 | 63.74 | 12.13 | 10.22 |
| Hy | 27.12 | 25.16 | 25.07 | 12.5 | 13.19 | 0.94 | 17.95 | 14.36 | 11.75 | 33.79 | 0.00 | 19.65 | 6.07 |
| Ol | 0 | 0 | 0 | 6.12 | 0 | 7.95 | 0 | 0 | 14.49 | 0 | 3.91 | 0.00 | 10.77 |
| Mag | 4.76 | 4.76 | 7.23 | 5.91 | 4.27 | 2.79 | 7.02 | 6.45 | 5.26 | 2.23 | 2.46 | 4.67 | 5.97 |
| Ilm | 2.69 | 5.03 | 2.95 | 4.01 | 2.73 | 1.38 | 2.59 | 2.95 | 1.36 | 1.05 | 0.30 | 2.47 | 1.39 |
| Ap | 0.52 | 0.52 | 0.45 | 1 | 0.12 | 0.08 | 0.38 | 0.76 | 0.11 | 0.1 | 0.07 | 0.33 | 0.19 |

**Appendix 1-C** Whole-rock analyses from metapelites in the Ongeva granulites.

| wt% | 23 | 28 | 29 | 601 | 621 | 701 | 709 | 728 | 757 | 784 | 807 | 822 | **average** |
|---|---|---|---|---|---|---|---|---|---|---|---|---|---|
| $SiO_2$ | 54.05 | 53.35 | 56.8 | 53.56 | 50.41 | 53.88 | 55.88 | 51.43 | 60.71 | 50.53 | 43.93 | 47.73 | 52.69 |
| $TiO_2$ | 0.78 | 0.78 | 0.68 | 1.05 | 1.13 | 0.88 | 0.69 | 1.04 | 1.06 | 0.87 | 1.04 | 0.66 | 0.89 |
| $Al_2O_3$ | 21.17 | 22.45 | 20.88 | 24.01 | 26.68 | 24.7 | 19.82 | 24.2 | 17.8 | 24.65 | 30.97 | 27.23 | 23.71 |
| $Fe_2O_3$ | 2.86 | 3.49 | 2.45 | 3.61 | 5.39 | 5.74 | 6.4 | 9 | 7.97 | 6.24 | 7.11 | 7.79 | 5.67 |
| FeO | 5.54 | 5.13 | 4.03 | 6.56 | 6.86 | 4.67 | 3.75 | 3.46 | 3.82 | 11.17 | 4.91 | 5.24 | 5.43 |
| MnO | 0.08 | 0.1 | 0.06 | 0.13 | 0.09 | 0.08 | 0.1 | 0.27 | 0.11 | 0.22 | 0.14 | 0.21 | 0.13 |
| MgO | 2.7 | 2.69 | 2.65 | 3.61 | 3.35 | 2.94 | 1.78 | 3.58 | 3.47 | 5.07 | 3.88 | 3.97 | 3.31 |
| CaO | 0.7 | 0.8 | 0.85 | 0.41 | 0.21 | 0.31 | 0.72 | 1.44 | 1.36 | 0.52 | 1.33 | 1.29 | 0.83 |
| $Na_2O$ | 1.45 | 1.33 | 2.32 | 0.78 | 0.32 | 0.57 | 1.63 | 0.28 | 0.66 | 0 | 0.75 | 1.34 | 0.95 |
| $K_2O$ | 9.52 | 8.21 | 7.8 | 5.2 | 4.25 | 5.1 | 8.49 | 4.25 | 2.39 | 0.17 | 4.22 | 3.26 | 5.24 |
| $P_2O_4$ | 0.07 | 0.06 | 0.06 | 0.04 | 0.02 | 0.04 | 0.06 | 0.03 | 0.03 | 0.03 | 0.05 | 0.05 | 0.05 |
| $H_2O^+$ | 0.63 | 0.96 | 0.86 | 0.76 | 0.91 | 0.8 | 0.61 | 0.72 | 0.56 | 0.65 | 1.62 | 0.71 | 0.82 |
| $H_2O^-$ | 0.03 | 0.07 | 0.05 | 0.15 | 0.15 | 0.15 | 0.15 | 0.2 | 0.14 | 0.1 | 0.13 | 0.09 | 0.12 |
| $CO_2$ | 0.04 | 0.19 | 0.09 | 0.09 | 0.07 | 0.16 | 0.16 | 0.31 | 0.2 | 0.07 | 0.22 | 0.39 | 0.17 |
| TOTAL | 99.63 | 99.6 | 99.59 | 99.96 | 99.84 | 100.04 | 100.24 | 100.2 | 100.29 | 100.29 | 100.31 | 99.96 | 99.99 |
| Trace elements (ppm) | | | | | | | | | | | | | |
| Ba | 693 | 867 | 1222 | 877 | 871 | 1023 | 1247 | 951 | 941 | 56 | 771 | 776 | 858 |
| Ce | 82 | 61 | 50 | 73 | 57 | 93 | 83 | 89 | 69 | 219 | 132 | 109 | 93 |
| Cr | 128 | 135 | 123 | 178 | 190 | 150 | 111 | 166 | 178 | 156 | 271 | 174 | 163 |
| Cu | 30 | 28 | 20 | 11 | 5 | 5 | 5 | 3 | 13 | 42 | 19 | 3 | 15 |
| Ga | 30 | 34 | 28 | 39 | 43 | 36 | 26 | 35 | 25 | 40 | 48 | 47 | 36 |
| La | 48 | 40 | 37 | 49 | 41 | 57 | 50 | 53 | 45 | 119 | 80 | 63 | 57 |
| Nb | 16 | 12 | 13 | 20 | 21 | 14 | 10 | 14 | 10 | 8 | 19 | 6 | 14 |
| Nd | 27 | 11 | 0 | 31 | 31 | 39 | 44 | 38 | 34 | 84 | 52 | 31 | 35 |
| Ni | 63 | 49 | 40 | 79 | 67 | 52 | 39 | 62 | 69 | 45 | 70 | 61 | 58 |
| Pb | 17 | 21 | 20 | 9 | 7 | 28 | 32 | 28 | 19 | 5 | 22 | 40 | 21 |
| Pr | 10 | 9 | 0 | 7 | 4 | 15 | 9 | 12 | 7 | 42 | 20 | 28 | 14 |
| Rb | 420 | 241 | 269 | 246 | 228 | 255 | 395 | 193 | 81 | 24 | 151 | 135 | 220 |
| Sr | 95 | 106 | 106 | 48 | 36 | 81 | 66 | 65 | 155 | 9 | 145 | 88 | 83 |
| Th | 23 | 8 | 7 | 20 | 14 | 24 | 19 | 27 | 20 | 78 | 35 | 31 | 26 |
| U | 4 | 2 | 2 | 0 | 1 | 0 | 0 | 0 | 1 | 1 | 2 | 1 | 1 |
| V | 143 | 121 | 95 | 157 | 158 | 137 | 96 | 113 | 108 | 140 | 193 | 139 | 133 |
| Y | 37 | 34 | 87 | 34 | 34 | 19 | 18 | 19 | 9 | 23 | 42 | 17 | 31 |
| Zn | 67 | 123 | 69 | 46 | 110 | 136 | 82 | 258 | 106 | 128 | 167 | 208 | 125 |
| Zr | 114 | 98 | 133 | 127 | 188 | 132 | 133 | 246 | 188 | 522 | 165 | 177 | 185 |